

# Search for the lepton flavor violating decay $A^0/H^0 \rightarrow \tau^\pm \mu^\mp$ at hadron colliders

Kétévi Adiklè Assamagan

Department of Physics, Brookhaven National Laboratory  
Upton, NY 11973 USA

Aldo Deandrea and Pierre-Antoine Delsart

Institut de Physique Nucléaire, Université de Lyon I  
4 rue E. Fermi, F-69622 Villeurbanne Cedex, France

## Abstract

In the two Higgs doublet model type III and in several other extensions of the Standard Model, there are no discrete symmetries that suppress flavor changing couplings at tree level. The experimental observation of the  $\nu_\mu - \nu_\tau$  flavor oscillation may suggest the non-conservation of lepton number. This would lead to the decay of the type  $A^0/H^0 \rightarrow \tau^\pm \mu^\mp$ . We determine the present low energy limit on lepton flavor violating (LFV) couplings from the muon  $g - 2$  measurement and discuss the prospects for detecting lepton flavor violating decays at the TeVatron and at the Large Hadron Collider. The achievable bounds on the LFV coupling parameter  $\lambda_{\tau\mu}$  are presented.

PACS: 12.60.Fr, 11.30.Hv, 14.80.Cp

LYCEN-2002-27  
BNL-69300  
ATL-COM-PHYS-2002-031  
July 2002

# Search for the lepton flavor violating decay $A^0/H^0 \rightarrow \tau^\pm \mu^\mp$ at hadron colliders

Kétévi A. Assamagan\*

*Department of Physics, Brookhaven National Laboratory, Upton, NY 11973 USA*

Aldo Deandrea<sup>†</sup> and Pierre-Antoine Delsart<sup>‡</sup>  
*Institut de Physique Nucléaire, Université Lyon I,  
4 rue E. Fermi, F-69622 Villeurbanne Cedex, France*  
(Dated: July, 2002)

In the two Higgs doublet model type III and in several other extensions of the Standard Model, there are no discrete symmetries that suppress flavor changing couplings at tree level. The experimental observation of the  $\nu_\mu\text{-}\nu_\tau$  flavor oscillation may suggest the non-conservation of lepton number. This would lead to the decay of the type  $A^0/H^0 \rightarrow \tau^\pm \mu^\mp$ . We determine the present low energy limit on lepton flavor violating (LFV) couplings from the muon  $g-2$  measurement and discuss the prospects for detecting lepton flavor violating decays at the TeVatron and at the Large Hadron Collider. The achievable bounds on the LFV coupling parameter  $\lambda_{\tau\mu}$  are presented.

PACS numbers: 12.60.Fr, 11.30.Hv, 14.80.Cp

## I. MOTIVATION

In the Standard Model (SM), lepton flavor is conserved separately for each generation. The diagonalization of the up-type and down-type mass matrices ensures the diagonalization of the Higgs-fermion coupling matrices [1]: the interaction term of the neutral fields in the SM can be written as:

$$\mathcal{L}_Y = -h_{ij}\bar{\psi}_i\psi_j\phi. \quad (1)$$

The spontaneous electro-weak symmetry breaking gives the mass matrix

$$M_{ij} = h_{ij} \langle \phi \rangle. \quad (2)$$

Diagonalizing  $M_{ij}$  also diagonalizes the Yukawa coupling matrix  $h_{ij}$ . The severe experimental limits on the existence of flavor changing neutral currents place stringent constraints on the flavor changing sector of extended models [2] where lepton flavor violation (LFV) may appear at tree level or may be induced at higher orders. In the Minimal Supersymmetric Standard Model (MSSM) the flavor problem is related to the soft supersymmetry breaking mass terms. In the basis where the lepton mass matrix is diagonalized, if there are non-zero off-diagonal matrix elements in the slepton mass matrix, LFV is introduced via loop contributions involving slepton mixing. There are many ways to avoid LFV, for example gravity [3] or gauge mediated [4] supersymmetry breaking, or flavor symmetries [5]. In the minimal super-gravity model (SUGRA) the supersymmetry breaking mass terms have a universal structure at a high scale of the order of the Planck scale. However LFV effects can be induced by

radiative corrections [6]. Large LFV effects can arise in supersymmetric models (SUSY) with a right-handed Majorana neutrino [7, 8, 9, 10] and in SUSY with R-parity violation [11].

In general, in models with several Higgs doublets, the up-type quarks and the down-type quarks can simultaneously couple to more than a single scalar doublet. As a result, the same operators do not diagonalize the mass matrices and the Higgs-fermion couplings, leading to the prediction of Flavor Changing Neutral Current (FCNC) at tree level. For instance in the two-Higgs Doublet Model (2HDM), the Yukawa interaction Lagrangian (for the neutral fields) can be written as:

$$\mathcal{L}_Y = -f_{ij}\bar{\psi}_i\psi_j\varphi_1 - g_{ij}\bar{\psi}_i\psi_j\varphi_2 \quad (3)$$

which gives, after spontaneous electro-weak symmetry breaking, a mass matrix of the form:

$$M_{ij} = f_{ij} \langle \varphi_1 \rangle + g_{ij} \langle \varphi_2 \rangle. \quad (4)$$

When this matrix  $M_{ij}$  is diagonalized, the coupling matrices  $f_{ij}$  and  $g_{ij}$  are not, in general, diagonalized. To suppress tree level FCNC in the theory so as not to be in conflict with known experimental limits, an *ad hoc* discrete symmetry is invoked [12] whereby the fermions of a given electric charge could couple to no more than one Higgs doublet. In the 2HDM, the up-type and the down-type quarks couple either to the same Higgs doublet (this is known as the 2HDM-I), or they could couple to different doublets (2HDM-II). One of the most stringent test of the 2HDM type I and type II comes from the measurement of the  $b \rightarrow s\gamma$  decay rate which receives substantial enhancement (over the SM prediction) in the 2HDM in a large region of the  $(m_{H^\pm}, \tan\beta)$  parameter space [13, 14, 15]. The measured  $b \rightarrow s\gamma$  decay rate from CLEO [16] and ALEPH [17] leads to a model dependent indirect lower bound of the charged Higgs mass as function of  $\tan\beta$  [18].

In the 2HDM-III, no discrete symmetries are present and in general FCNC exist in this model [19, 20]. As

\*Electronic address: ketevi@bnl.gov

<sup>†</sup>Electronic address: deandrea@ipnl.in2p3.fr

<sup>‡</sup>Electronic address: delsart@ipnl.in2p3.fr

an example the LFV interaction Lagrangian of the light neutral Higgs boson  $h$  of the 2HDM-III type b (see the Appendix for details) is:

$$-\mathcal{L}_{LFV} = h_{ij} \bar{l}_i l_j h + \text{h.c.} = \xi_{ij} \frac{\cos(\alpha - \beta)}{\sqrt{2} \cos \beta} \bar{l}_i l_j h + \text{h.c.} \quad (5)$$

where  $\alpha$  is the mixing angle of the neutral Higgs sector and  $\xi_{ij}$  the Yukawa LFV couplings and  $i, j$  are the generation indices (in the following the notation  $h_{ij}$  will be used to indicate the generic Yukawa coupling including the mixing angles). To be consistent with experimental data on  $K^0 - \bar{K}^0$ ,  $D^0 - \bar{D}^0$  and  $B^0 - \bar{B}^0$  mixing which put stringent constraints on flavor changing couplings with the first generation index, and since one might expect the biggest contribution to come from the LFV couplings of the second and the third generation ( $\xi_{sb}$ ,  $\xi_{\tau\mu}$ ,  $\xi_{ct}$ ), these couplings have been parameterized as a function of the masses of the fermions involved since a natural hierarchy is found in the fermion masses [2]:

$$\xi_{ij} = \lambda_{ij} \frac{\sqrt{m_i m_j}}{v}, \quad (6)$$

where  $v \simeq 246$  GeV and the residual arbitrariness of flavor changing couplings is expressed by the parameters  $\lambda_{ij}$  which is constrained by experimental bounds on FCNC and LFV processes. A similar hierarchy will be assumed for the LFV coupling  $\eta_{ij}$  of 2HDM-III type a — see the appendix. In the charged Higgs decays this implies a zero LFV coupling if the neutrino is massless and in general a suppression proportional to the square root of the small neutrino mass. We also consider an alternative case in which we drop the neutrino mass dependence for the charged Higgs LFV couplings and adopt instead the same parameterization as in the neutral Higgs sector. In the numerical analysis of the muon anomalous magnetic moment, this distinction is not important as the charged Higgs contribution is small in both cases and can be neglected in comparison to the neutral ones for the range of masses and mixing angles considered.

## II. LOW ENERGY BOUNDS

In the purely leptonic sector, the  $\mu \rightarrow e\gamma$  conversion process gives  $\sqrt{\lambda_{\tau\mu}\lambda_{e\tau}} < 5$  [21]. It would be desirable to examine a process that depends only on a single coupling. One such process is the muon anomalous magnetic moment  $a_\mu = (g_\mu - 2)/2$  [22] where high precision data [23] can be used to constrain  $\lambda_{\tau\mu}$ , by comparing the measured  $a_\mu$  to the theoretical prediction of the SM. The new experimental world average reads [23]:

$$a_\mu^{\text{exp}} = 11659203(8) \times 10^{-10}. \quad (7)$$

Recently, the standard model calculation was revised in order to take into account the correct sign for the light by

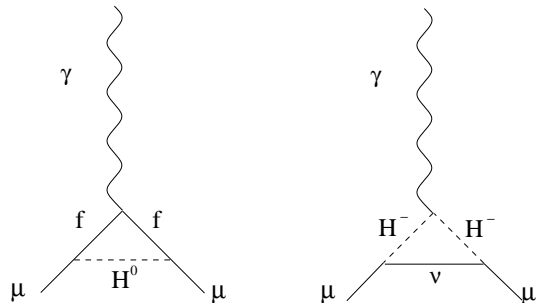


FIG. 1: The one-loop contributions of the Higgs sector to  $a_\mu$ .  $H^0$  stands for a generic neutral Higgs boson,  $f$  is a lepton. With  $f = \mu$  we obtain the flavor conserving contribution, with  $f = \tau$  the LFV one. As explained in the text we neglect the LFV contribution with  $f = e$ .

light hadronic contribution [24] and the standard model expectation is :

$$a_\mu^{\text{SM}} = 11659177(7) \times 10^{-10}. \quad (8)$$

Another often quoted value is

$$a_\mu^{\text{SM}} = 11659186(8) \times 10^{-10} \quad (9)$$

which gives only slightly more restrictive figures if used to bound the LFV couplings. In the following we shall use the value of Equation (8). Note that a recent evaluation of the light by light hadronic correction [25] based on chiral perturbation theory suggests that the theoretical error due to unknown low energy constants from sub-leading contributions may increase the estimated error. The difference between experiment and the SM theoretical calculation is:

$$\Delta a_\mu = a_\mu^{\text{exp}} - a_\mu^{\text{SM}} = 26(11) \times 10^{-10}. \quad (10)$$

We obtain the 90% confidence level (CL) range on  $\Delta a_\mu$

$$8 \times 10^{-10} \leq \Delta a_\mu \leq 44 \times 10^{-10} \quad (11)$$

to constrain new physics. In the following we shall consider the effect of flavor violating Higgs-leptons interactions plus the flavor conserving Higgs bosons contributions as the only additional ones with respect to the SM. At one-loop level the Feynman diagrams are those of Figure 1 and the contribution to  $a_\mu$  is given for a large class of models by [26] (see also the erratum in [1] concerning other results in the literature), and can be used to obtain the one-loop Higgs contributions to  $a_\mu$  for the model considered in this paper:

$$\Delta a_\mu^N = \frac{h_{\mu f}^2 m_\mu^2}{8\pi^2} \int_0^1 \frac{x^2(1-x) \pm x^2(m_f/m_\mu)}{m_\mu^2 x^2 + x(m_f^2 - m_\mu^2) + (1-x)m_H^2} dx \quad (12)$$

for a neutral Higgs boson and the sign is  $+$ ( $-$ ) for the scalar (pseudo-scalar).  $h_{ij}$  is here a generic Yukawa coupling, whose expression in terms of  $\eta_{ij}$  or  $\xi_{ij}$  and the

angles  $\alpha$ ,  $\beta$  can be read in the Lagrangian given in the appendix.  $m_f$  is the mass of the muon for the flavor conserving contribution with coupling  $h_{\mu\mu}$ , and  $m_f = m_\tau$  for the LFV contribution with coupling  $h_{\mu\tau}$ . We neglect the electron contribution as the coupling  $h_{\mu e}$  is more constrained and because of the natural hierarchy assumed in formula (6). For the charged Higgs boson we have the same coupling for the scalar and pseudoscalar contributions in the Lagrangian, therefore we give the sum of the two in one formula:

$$\Delta a_\mu^C = \frac{h_{\mu\nu}^2 m_\mu^2}{8\pi^2} \int_0^1 \frac{2x^2(x-1)}{m_\mu^2 x^2 + x(m_H^2 - m_\mu^2)} dx \quad (13)$$

where we neglected terms proportional to the neutrino mass. In order to give the bounds coming from the  $g-2$  measurement we choose the sets of mass and mixing angle parameters of Table I. By calculating the contribution

TABLE I: The four sets of parameters used to obtain bounds on the LFV couplings. Set 1–3 are consistent with the relations between masses and mixing angles obtained at one-loop within the MSSM [27] in order to allow for a comparison. Note however that the 2HDM-III is not constrained by the symmetries imposed on MSSM in order to avoid tree-level LFV. Set 4 corresponds to a choice of parameters that is not allowed in MSSM. Masses are in GeV and the angle  $\alpha$  in rad.

Set	$m_h$	$m_H$	$m_A$	$m_{H^\pm}$	$\alpha$	$\tan\beta$
(1)	93	134	100	127	0.4	5
(2)	127	131	129	160	-0.58	45
(3)	128	500	496	509	0	50
(4)	125	200	200	250	0.2	10

to  $a_\mu$  from the Higgs sector we obtain limits on the LFV couplings of 2HDM-III type a and b — we use only the upper limits of (11) to derive the muon  $g-2$  bounds on the LFV couplings. The results are in Table II. In

TABLE II: The 90% CL limits on the LFV couplings  $\lambda_{\tau\mu}$ ,  $\xi_{\tau\mu}$ ,  $\eta_{\tau\mu}$  from the experimental measurement of  $a_\mu$ .

Set	2HDM-III type a	2HDM-III type b
(1)	$\lambda_{\tau\mu} < 31$ ( $\eta_{\tau\mu} < 0.06$ )	$\lambda_{\tau\mu} < 6.3$ ( $\xi_{\tau\mu} < 0.012$ )
(2)	$\lambda_{\tau\mu} < 38$ ( $\eta_{\tau\mu} < 0.07$ )	$\lambda_{\tau\mu} < 0.8$ ( $\xi_{\tau\mu} < 0.002$ )
(3)	$\lambda_{\tau\mu} < 123$ ( $\eta_{\tau\mu} < 0.24$ )	$\lambda_{\tau\mu} < 2.5$ ( $\xi_{\tau\mu} < 0.005$ )
(4)	$\lambda_{\tau\mu} < 53$ ( $\eta_{\tau\mu} < 0.10$ )	$\lambda_{\tau\mu} < 5.3$ ( $\xi_{\tau\mu} < 0.010$ )

Figure 2 we show the values of  $\Delta a_\mu$  given by the 2HDM-III using the set (2) of parameters of Table I with  $\lambda_{\mu\nu} = 10$  as a function of  $\tan\beta$ . In model type a,  $\Delta a_\mu$  is almost flat for  $\tan\beta > 2$ , while in model type b it is a growing function of  $\tan\beta$ . The same is true for the other sets of parameters. In both models the Higgs sector contribution to  $\Delta a_\mu$  is a growing function of the LFV couplings.

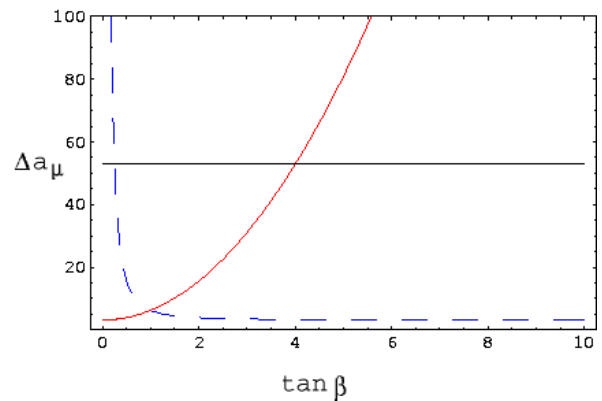


FIG. 2:  $\Delta a_\mu$  in units of  $10^{-10}$  as a function of  $\tan\beta$  using set 2 of parameters for the 2HDM-III type a (dashed line) and 2HDM-III type b (continuous line). The region above the horizontal line is excluded at 90 % CL by the muon  $g-2$  data.

### III. COLLIDER EXPERIMENTS

Bounds on other LFV couplings  $\lambda_{ij}$  can be obtained from the processes  $B_s \rightarrow \mu\mu$ ,  $B \rightarrow X_s \mu\mu$ ,  $e^+e^- \rightarrow \bar{t}c\nu_e\bar{\nu}_e$ ,  $e^+e^- \rightarrow tt\bar{c}\bar{c}$ ,  $\mu^+\mu^- \rightarrow tc$ ,  $B_s \rightarrow (K)\tau\mu$  and  $B_s \rightarrow (K)\tau\tau$  [19]. However, the bounds obtained from these processes would involve two couplings as in the case of  $\mu \rightarrow e\gamma$ . The flavor changing process  $t \rightarrow H^0 c$  has been extensively studied for the LHC [28]; in the context of the 2HDM-I and II, top quark decays beyond the SM,

$$t \rightarrow ch \quad (h = h^0, H^0, A^0), \quad (14)$$

were studied in [29] and it is shown that these processes could be accessible at the LHC and at the linear collider; the prospects for detecting the decay  $t \rightarrow cH$  at the  $e^+e^-$  linear collider have also been investigated in [30].

The  $\nu_\mu - \nu_\tau$  flavor mixing observed in the atmospheric neutrino experiments [31] would lead to the flavor violating decays

$$\tau^\pm \rightarrow \mu^\pm \gamma, \quad (15)$$

$$\tau^\pm \rightarrow \mu^\pm \mu^+ \mu^-, \quad (16)$$

$$\tilde{\chi}_2^0 \rightarrow \tilde{\chi}_1^0 \tau \mu, \quad (17)$$

$$h \rightarrow \tau^\pm \mu^\mp. \quad (18)$$

SUSY can accommodate the observed flavor mixing [8, 9, 10] and thus, the LFV processes (15), (16) and (17) would arise in these models. A study conducted at the LHC showed that an upper bound of  $0.6 \times 10^{-6}$  on the  $\tau^\pm \rightarrow \mu^\pm \gamma$  branching ratio can be achieved with an integrated luminosity of  $30 \text{ fb}^{-1}$  while theoretical estimates are at the level of  $10^{-9}$  or less [10, 32]. Direct evidence of LFV in the slepton sector of SUSY would be inferred in the observation of the process (17) which has also been studied for the LHC [33]. It was shown that in some

cases, the direct evidence would offer better sensitive than the  $\tau^\pm \rightarrow \mu^\pm \gamma$  process.

The decay  $h \rightarrow \tau^\pm \mu^\mp$  can be accommodated in the 2HDM-III where no discrete symmetry suppresses the LFV couplings at tree level, and the partial decay width is parameterized by the LFV coupling  $\lambda_{\tau\mu}$ . The decay  $H^0 \rightarrow l_i^+ l_i^-$  (SM-like) will be used in the following as a comparison for the LFV decays. Its partial width is

$$\Gamma_{SM}(H^0 \rightarrow l_i^+ l_i^-) = m_H \frac{1}{8\pi} \frac{m_i^2}{v^2}, \quad (19)$$

where we neglect small terms of the type  $m_i/m_H$  — see the appendix for complete expressions. The partial width of the decay  $H^0 \rightarrow l_i^\pm l_j^\mp$  (where  $l = e, \mu, \tau$  and  $i \neq j$ ) is for 2HDM-III type a

$$\Gamma(H^0 \rightarrow l_i^\pm l_j^\mp) = m_H \frac{\lambda_{ij}^2}{8\pi} \frac{m_i m_j}{v^2} \frac{\sin^2(\alpha - \beta)}{2 \sin^2 \beta} \quad (20)$$

and

$$\Gamma(H^0 \rightarrow l_i^\pm l_j^\mp) = m_H \frac{\lambda_{ij}^2}{8\pi} \frac{m_i m_j}{v^2} \frac{\sin^2(\alpha - \beta)}{2 \cos^2 \beta} \quad (21)$$

for 2HDM-III type b.

Hadron colliders may be sensitive to the processes  $h \rightarrow e^\pm \mu^\mp$  and  $h \rightarrow \tau^\pm e^\mp$  [34], particularly at high luminosity, but these decays are not considered in the present study which is further motivated by a favorable interpretation of the atmospheric neutrino mixing experiments. It is shown in [35] that the muon collider would be sensitive to  $H^0 \rightarrow \tau^\pm \mu^\mp$ . The non-observation of this process for  $m_H < 140$  GeV at the muon collider in addition to the failure to detect the top quark decay  $t \rightarrow cH^0$  at the LHC [28] would rule out the 2HDM-III [35].

In this paper, we present the prospects for the detection of the LFV decay  $A^0/H^0 \rightarrow \tau^\pm \mu^\mp$  at the LHC and TeVatron. We shall consider the 2HDM-III and we shall parameterize the  $A^0/H^0 \rightarrow \tau^\pm \mu^\mp$  branching ratio ( $BR$ ) by the LFV coupling parameter  $\kappa_{\tau\mu}$  [36] with respect to the SM-like decay  $H^0 \rightarrow \tau^+ \tau^-$  given in formula (19):

$$BR(A^0/H^0 \rightarrow \tau\mu) = \kappa_{\tau\mu}^2 \left( \frac{2m_\mu}{m_\tau} \right) BR_{SM}(H^0 \rightarrow \tau\tau) \quad (22)$$

where the dependence on  $\alpha, \beta$ , the ratio of the total widths and  $\lambda_{\tau\mu}$  is absorbed into the LFV coupling parameter  $\kappa_{\tau\mu}$ . For example, for the decay and the model considered in formula (20) we have:

$$\kappa_{\tau\mu} = \lambda_{\tau\mu} \frac{\sin(\alpha - \beta)}{\sqrt{2} \sin \beta} \sqrt{\frac{\Gamma_T^{SM}}{\Gamma_T^a}} \quad (23)$$

while from formula (21) we obtain:

$$\kappa_{\tau\mu} = \lambda_{\tau\mu} \frac{\sin(\alpha - \beta)}{\sqrt{2} \cos \beta} \sqrt{\frac{\Gamma_T^{SM}}{\Gamma_T^b}} \quad (24)$$

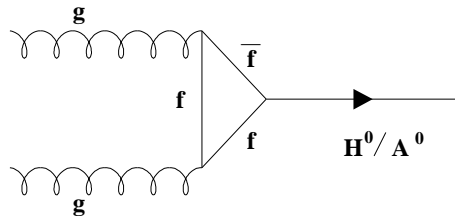


FIG. 3: Higgs boson production mechanism through gluon fusion.

where  $\Gamma_T^{SM}$  is the total SM-like width and  $\Gamma_T^{a,b}$  is the total width in model  $a, b$  respectively. Similar formulas can be written for the  $h^0$  and  $A^0$  Higgs bosons. For  $h^0$  one has to replace  $\sin(\alpha - \beta)$  in equations (23) and (24) with  $\cos(\alpha - \beta)$ . For  $A^0$  one has to replace  $\sin(\alpha - \beta)$  with 1.

In Table III we give examples of the correspondence between the parameterization in terms of  $\lambda$  and the one in terms of  $\kappa$  for set 1 and set 2 of Table I.

TABLE III: The correspondence between the parameters  $\kappa$  and  $\lambda$  using set 1 (set 2) of Table I for the LFV couplings of the Higgs bosons  $H^0$  and  $A^0$ .

	$\lambda = 1$	$\lambda = 5$	$\lambda = 10$
type a			
$\kappa(H^0)$	1.1 (1.2)	9.4 (6.2)	7.8 (12.2)
$\kappa(A^0)$	3.3 (30.7)	16.6 (68)	7 (72.6)
type b			
$\kappa(H^0)$	1.1 (0.7)	5 (3.3)	7.6 (6.5)
$\kappa(A^0)$	0.1 (0.001)	0.5 (0.006)	1 (0.01)

We shall discuss the achievable bounds on  $\kappa_{\tau\mu}$  and  $\lambda_{\tau\mu}$  in the following sections.

#### IV. SEARCH FOR $A^0/H^0 \rightarrow \tau\mu$

We consider the production of the neutral Higgs bosons  $A^0$  and  $H^0$  through gluon fusion,  $gg \rightarrow A^0/H^0$  (see Figure 3), and the LFV decay  $A^0/H^0 \rightarrow \tau^\pm \mu^\mp$  (Figure 4). We restrict the present work to the low mass region,  $120 < m_A < 160$  GeV, primarily because the SM decay  $H_{SM}^0 \rightarrow \tau^+ \tau^-$ , hence  $A^0/H^0 \rightarrow \tau^+ \mu^-$  — see Equation (22) — becomes negligible [37] as the SM mode  $H_{SM}^0 \rightarrow W^+ W^-$  opens up around 160 GeV as shown in Figure 5 where we assume  $\kappa_{\tau\mu} = 1$ . We take as a reference the parameters of set 2 in Table I for comparison with the MSSM case without loss of generality. The events are generated in PYTHIA6.2 [38] with CTEQ5L [39] parton distribution function parameterization, and with the detector resolution and efficiencies parameterization of ATLFast [40] from full detector simulations.

We search for a final state where the  $\tau$  lepton decays to hadrons,  $\tau \rightarrow \text{jet } \nu_\tau$  with a branching ratio of

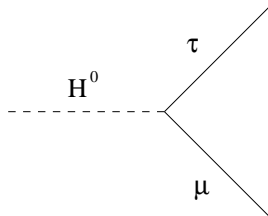


FIG. 4: The Higgs decay through the lepton flavor violating coupling  $H^0 \tau \mu$ .

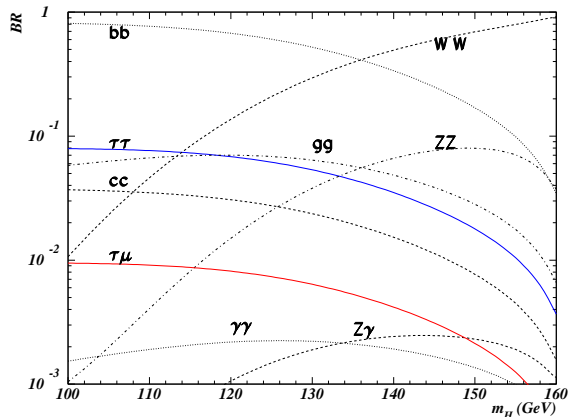


FIG. 5: The Higgs boson decay branching ratios as a function of  $m_H$ . For the  $A^0/H^0 \rightarrow \tau^+ \mu^- + \tau^- \mu^+$  channel, the coupling parameter  $\kappa_{\tau\mu}$  is taken to be one.

$\sim 65\%$  or to an electron,  $\tau \rightarrow e\nu_e\nu_\tau$  ( $BR \sim 18\%$ ). The main backgrounds — in both final states — include the  $W^+W^-$  pair production, the Drell-Yan type process  $Z^0(\gamma^*) \rightarrow \tau^+\tau^-$ . For the hadronic  $\tau$  decays, an additional background comes from  $W^\pm$ +jets events where a jet is mis-identified as a  $\tau$  jet:

$$\begin{aligned}
 pp(\bar{p}) \rightarrow & W^\pm Z^0 \rightarrow \mu^\pm \nu_\mu \tau^+ \tau^-, & (25) \\
 \rightarrow & W^+W^- \rightarrow \mu^+ \nu_\mu \tau^- \bar{\nu}_\tau, \\
 \rightarrow & t\bar{t} \rightarrow \mu^\pm \nu_\mu b\tau^\mp \nu_\tau \bar{b}, \\
 \rightarrow & Z^0(\gamma^*) \rightarrow \tau^+\tau^- \rightarrow \mu^+ \nu_\mu \bar{\nu}_\tau \tau^-, \\
 \rightarrow & W^\pm + \text{jets} \rightarrow \mu^\pm \nu_\mu + \text{jets}.
 \end{aligned}$$

The  $gg \rightarrow A^0/H^0$  cross sections are calculated using the program HIGLU [41]. The signal cross-sections have been calculated at next-to-leading order (NLO) and next-next-to-leading order (NNLO) [41, 42]. For the backgrounds, NLO estimates are available [43, 44, 45], except for  $W^\pm$ +jets where NLO calculations have been performed for a vector boson production with 2 jets at the TeVatron [46]. We have therefore used the leading order (LO) estimates of the signal and background cross sections.

Unless explicitly stated otherwise, the normalizations

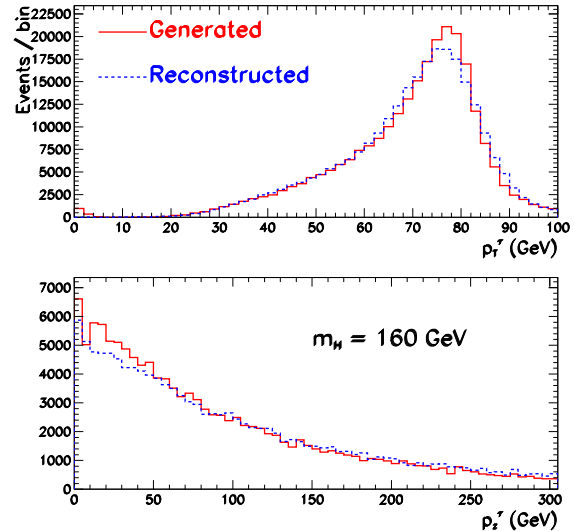


FIG. 6: The reconstructed and the generated  $p_T$  (top plot) and  $p_z$  (bottom plot) of the  $\tau$  lepton. Equations (26) are used for the reconstructed quantities.

of the figures referenced in the sections IV A–IV C are that of three years at low luminosity for one experiment at the LHC using the rates shown in Table IV.

### A. Hadronic $\tau$ decay

The event selection for the hadronic final state of the  $\tau$  lepton is carried as described below:

- (1) Search for one isolated muon ( $p_T^\mu > 20$  GeV,  $|\eta^\mu| < 2.5$ ) to provide the experimental trigger, and one hadronic  $\tau$  jet ( $p_T^\tau > 20$  GeV,  $|\eta^\tau| < 2.5$ ). We further require a jet veto and a b-jet veto — no other jet with  $p_T > 20$  GeV within  $|\eta| < 2.5$  — to reduce  $W^\pm$ +jets and  $t\bar{t} \rightarrow \bar{b}\mu^+\nu_\mu b\tau^-\bar{\nu}_\tau$  backgrounds. A  $\tau$  jet identification efficiency of 30% is assumed.
- (2) The 4-momentum of the  $\tau$  lepton is reconstructed from the  $\tau$  jet and the missing transverse momentum (using the prescription of [48]) as follows:

$$\begin{aligned}
 \vec{p}_T^\tau &= \vec{p}_T^{\tau\text{-jet}} + \vec{p}_T^{\text{miss}}, & (26) \\
 p_z^\tau &= p_z^{\tau\text{-jet}} \left( 1 + \frac{p_T^{\text{miss}}}{p_T^{\tau\text{-jet}}} \right), \\
 E_\tau^2 &= \vec{p}_\tau^2 + m_\tau^2.
 \end{aligned}$$

The reconstructed momenta of the  $\tau$  lepton using Equations (26) are shown in Figure 6 together with the generated momenta. We demand that the hadronic  $\tau$  jet carries at least 60% of the  $\tau$  lepton

TABLE IV: The rates,  $\sigma \times \text{BR}(\text{pb})$ , for the signal  $gg \rightarrow A^0/H^0 \rightarrow \tau^+\mu^- + \tau^-\mu^+$ , and the backgrounds at the LHC. The dominant backgrounds are  $Z \rightarrow \tau\tau$  and  $W^\pm + \text{jets}$  where  $W^\pm \rightarrow \mu^\pm\nu_\mu$  and a jet is mis-identified as a  $\tau$  jet. We assume the coupling parameter  $\kappa_{\tau\mu} = 1$  and  $\tan\beta = 45$  in the estimate of the signal rates. An additional background comes  $gg \rightarrow A^0/H^0 \rightarrow \tau^+\tau^-$  with one  $\tau$  decaying to  $\mu$ ,  $\tau \rightarrow \mu\nu_\mu\nu_\tau$  and the other  $\tau$  decays to hadrons. At  $\tan\beta = 45$ , the scalar and the pseudo-scalar Higgs bosons are degenerate in mass for  $m_A \geq 130$  GeV, and the relative strengths of  $gg \rightarrow A^0 \rightarrow \tau\mu$  and  $gg \rightarrow H^0 \rightarrow \tau\mu$  are not important. For  $m_A = 120$  GeV, the  $A^0$  and the  $H^0$  bosons have comparable strengths.

Process	$m_A$ (GeV)	$m_H$ (GeV)	$\sigma \times \text{BR}(\text{pb})$
$gg \rightarrow A^0/H^0 \rightarrow \tau^+\mu^- + \tau^-\mu^+$	119.3	128.4	7.5
	129.3	130.1	4.5
	139.2	140.2	2.1
	149.1	150.0	0.8
	159.1	160.0	0.1
$gg \rightarrow A^0/H^0 \rightarrow \tau\tau$	119.3	128.4	99.5
	129.3	130.1	76.4
	139.2	140.2	54.3
	149.1	150.0	39.0
	159.1	160.0	28.5
$pp \rightarrow W^\pm Z^0 \rightarrow \mu^\pm\nu_\mu\tau^+\tau^-$		0.2	
$pp \rightarrow W^+W^- \rightarrow \mu^+\nu_\mu\tau^-\bar{\nu}_\tau$		1.67	
$pp \rightarrow t\bar{t} \rightarrow \mu^\pm\nu_\mu b\tau^\pm\nu_\tau\bar{b}$		$1.37 \cdot 10^1$	
$pp \rightarrow Z^0(\gamma^*) \rightarrow \tau^+\tau^- \rightarrow \mu^+\nu_\mu\bar{\nu}_\tau\tau^-$		$1.39 \cdot 10^4$	
$pp \rightarrow W^\pm + \text{jets} \rightarrow \mu^\pm\nu_\mu + \text{jets}$		$1.75 \cdot 10^4$	

energy and the cone  $\Delta R = \sqrt{\Delta\eta^2 + \Delta\phi^2}$  between the  $\tau$  jet axis and the  $\tau$  lepton direction be less than 0.2 rad:

$$\frac{p_T^{\tau\text{-jet}}}{p_T^\tau} > 0.6, \quad (27)$$

$$\Delta R(p_T^{\tau\text{-jet}}, p_T^\tau) < 0.2 \text{ rad.}$$

This cut reduces the background from  $W^\pm + \text{jets}$  events by more than one order of magnitude while it costs only a modest  $\sim 40\%$  rejection of signal events.

- (3) Using the tracker information in the off-line  $\tau$  identification, we require that the  $\tau$  jet candidate contains a single charged track within  $\Delta R < 0.3$  rad around the jet axis. This cut would select one prong hadronic  $\tau$  decay events, and as shown in Figure 7, it reduces the  $W^\pm + \text{jets}$  events by an additional factor of ten while costing only  $\sim 50\%$  reduction in the signal reconstruction efficiencies.
- (4) The  $\tau$  lepton from the signal is ultra-relativistic, and as a result, the missing momentum from  $\tau \rightarrow (\tau\text{jet})\nu$  is collinear with the  $\tau$  jet. Further, as a consequence of the two-body decay, the  $\tau$  jet and the  $\mu$  track are back-to-back. We therefore require a large azimuthal opening angle between the  $\mu$  and the  $\tau$  jet and a small opening angle between  $p_T^{\text{miss}}$  and the  $\tau$  jet:

$$\delta\phi(p_T^\mu, p_T^{\tau\text{-jet}}) > 2.75 \text{ rad}, \quad (28)$$

$$\delta\phi(p_T^{\text{miss}}, p_T^{\tau\text{-jet}}) < 0.6 \text{ rad.}$$

As can be seen from Figure 8, this cut reduces the signal by  $\sim 35\%$  while the  $pp(\bar{p}) \rightarrow Z^0(\gamma^*)$  background is further suppressed by  $\sim 51\%$ .

- (5) The  $\mu$  track is mono-energetic because of the two-body decay  $H^0 \rightarrow \tau^\pm \mu^\mp$  but the  $\tau$  jet in  $\tau \rightarrow (\tau\text{jet})\nu$  would be somewhat softer. As a result, one would expect the momentum difference

$$\Delta p_T = p_T^\mu - p_T^{\tau\text{-jet}} \quad (29)$$

to be positive for the signal. Indeed, as noted in [48] and as shown in Figure 9, this quantity is very powerful in suppressing the  $pp(\bar{p}) \rightarrow Z^0(\gamma^*)$  background further.

- (6) We now cut on the transverse momentum of the  $\tau$  reconstructed according to Equations (26). The distribution of this variable is shown in Figure 10 where one sees that demanding  $p_T^\tau > 50$  GeV leads to at most 20% reduction in the signal — the  $\tau$  gets harder at higher  $m_A$  so the reduction in the signal due to this cut is highest at the lowest mass considered, i.e.,  $m_A = 120$  GeV — while the  $W^\pm + \text{jets}$  and  $Z^0(\gamma^*) \rightarrow \tau^+\tau^-$  backgrounds are suppressed by additional factors of two and ten respectively.

- (7) The effective transverse mass of the  $\tau\mu$  system

$$m_T = \sqrt{2p_T^\mu p_T^{\tau\text{-jet}} [(1 - \cos\delta\phi)]} \quad (30)$$

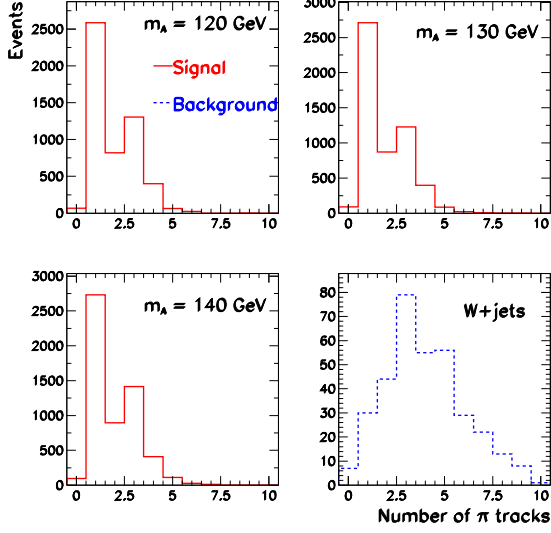


FIG. 7: The number of reconstructed charged tracks (arbitrary normalization) within  $\Delta R < 0.3$  rad of the calorimeter jet axis. By requiring a single reconstructed charged track so as to select one prong  $\tau$  decays, the  $W^\pm$ +jets background is further reduced by one order of magnitude while the signal suffers  $\sim$  factor of two reduction consistent with the one prong hadronic  $\tau$  decay branching fraction.

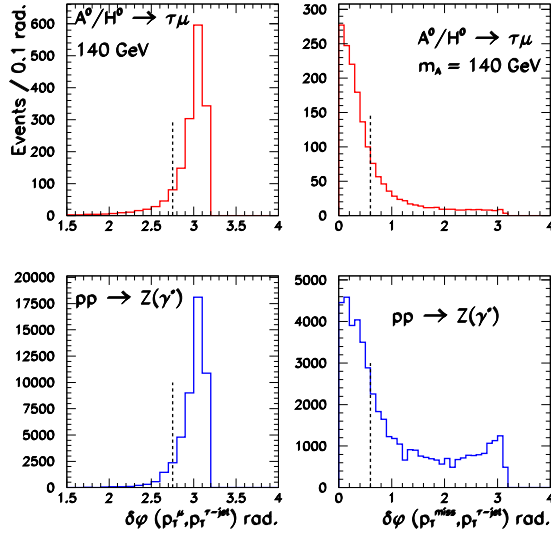


FIG. 8: The azimuthal opening angle  $\delta\phi$  between the muon track and the  $\tau$  jet (left plots), and between the  $p_T^{\text{miss}}$  vector and the  $\tau$  jet (right plots). The  $pp(\bar{p}) \rightarrow Z^0(\gamma^*)$  background is further reduced by a factor of two while the signal suffers only a 35% reduction. The dashed lines indicate the level of the cuts.

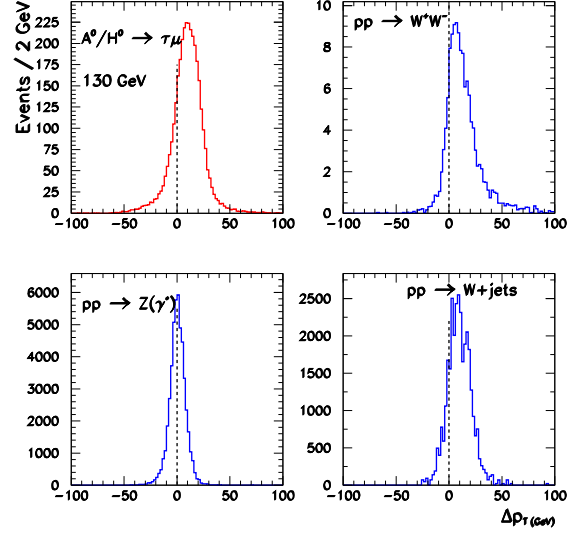


FIG. 9: The momentum imbalance  $\Delta p_T$  between the muon track and the  $\tau$  jet. In the signal, this quantity is expected to be positive as a result of the two-body kinematics from  $A^0/H^0 \rightarrow \tau^\pm \mu^\mp$  and the subsequent decay  $\tau \rightarrow (\tau \text{ jet})\nu$ . This is indeed mostly the case as shown in the top left plot. Therefore, demanding  $\Delta p_T > 0$  suppresses the backgrounds further, particularly the Drell-Yan type process  $pp(\bar{p}) \rightarrow Z^0(\gamma^*)$  which is reduced by as much as 50% with this cut alone as can be seen from the bottom left plot.

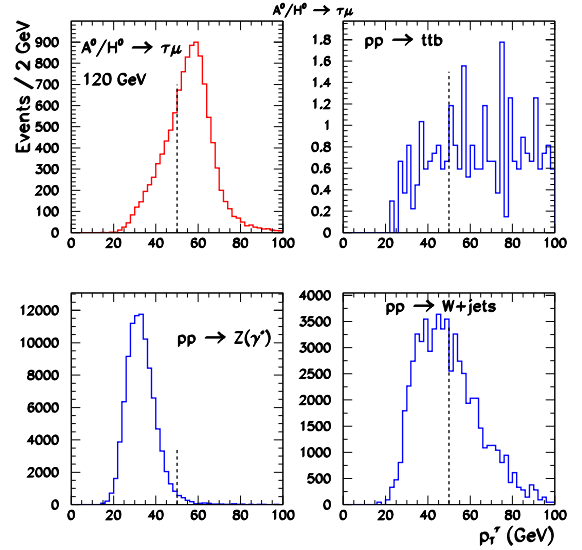


FIG. 10: The reconstructed transverse momentum of the  $\tau$  lepton. We require that this quantity be greater 50 GeV leading to additional suppression factors of two and ten in the dominant  $W^\pm$ +jets and  $Z^0(\gamma^*) \rightarrow \tau^+\tau^-$  backgrounds whereas the signal is reduced by at most 20%.



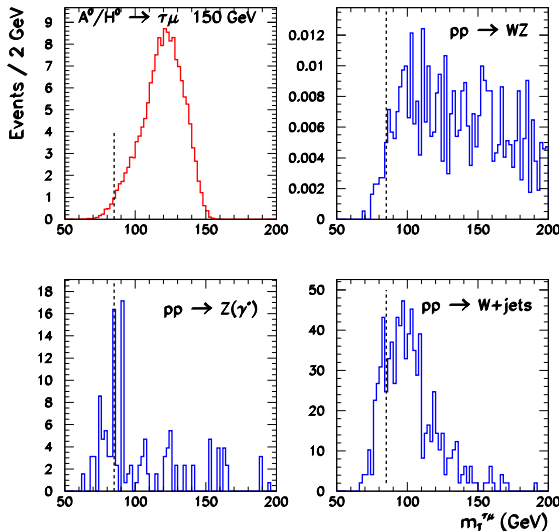


FIG. 11: The reconstructed effective transverse mass of the  $\tau\mu$  system. This distribution peaks at low values in the backgrounds while in signal the peak is closer to the actual Higgs mass. The dashed lines indicate the cut applied on this quantity.

is reconstructed. In the signal, one would expect this quantity to peak toward the Higgs mass whereas in the backgrounds, because the final state may contain several neutrinos, the  $m_T$  distribution would peak at low values as shown in Figure 11. We required that  $m_T > 85$  GeV. This cut suppresses the  $Z^0(\gamma^*) \rightarrow \tau^+\tau^-$  background more than the other backgrounds.

The efficiencies of the cuts discussed above are shown in Table V where one sees that the analysis steps described here is effective in reducing the two main backgrounds namely  $W^\pm$ +jets and  $Z^0 \rightarrow \tau^+\tau^-$ . The most effective cuts are the ones imposed for the identification of the  $\tau$  lepton — cuts (2) and (3) — and some kinematic cuts such as the momentum imbalance defined in cut (5).

With the  $\tau$  4-momentum  $p^\tau$  obtained in Equations (26), the invariant mass of the Higgs boson is reconstructed,

$$m_{\tau\mu}^2 = (p^\tau + p^\mu)^2. \quad (31)$$

Distributions of  $m_{\tau\mu}$  are shown in Figure 12 for the signal and the backgrounds. We see in this figure that the signal is reconstructed within one GeV of the expected Higgs boson mass — except at  $m_A = 120$  GeV where the  $A^0$  and the  $H^0$  are not degenerate in mass and their summed signal peaks somewhere in the middle — while in the backgrounds the  $m_{\tau\mu}$  distribution gives a continuum spectrum dominated by  $W^\pm$ +jets event.

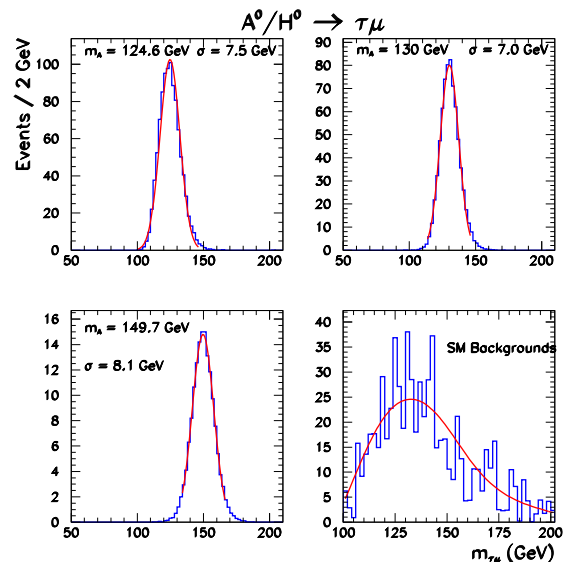


FIG. 12: The invariant mass  $m_{\tau\mu}$  distributions of the signal  $A^0/H^0 \rightarrow \tau^\pm\mu^\mp$  for several values of the Higgs boson mass and also of the backgrounds, after an integrated luminosity of  $30 \text{ fb}^{-1}$ . The LFV coupling parameter  $\kappa_{\tau\mu}^2 = 1$ . The signal is reconstructed to within 5 GeV of the Higgs mass above the residual  $W^\pm$ +jets continuum.

### B. $A^0/H^0 \rightarrow \tau^\pm\mu^\mp$ versus $A^0/H^0 \rightarrow \tau^+\tau^-$

The  $H^0 \rightarrow \tau^+\tau^-$  of the SM is not expected to yield a significant signal at the LHC due to a low signal rate and substantial backgrounds from various sources [49]. In the MSSM, for a Higgs boson of the same mass, the  $A^0/H^0 \rightarrow \tau^+\tau^-$  rates are significantly larger than the SM case. The  $A^0/H^0 \rightarrow \tau^+\tau^-$  process has been studied extensively for the LHC, and it is demonstrated that such a signal can be observed with a significance exceeding  $5\sigma$  in a large area of the  $(m_A, \tan\beta)$  plane [50, 51].

The final state of both processes  $A^0/H^0 \rightarrow \tau^+\tau^-$  and  $A^0/H^0 \rightarrow \tau^\pm\mu^\mp$  are very similar, namely an isolated  $\mu$ , a hadronic  $\tau$  jet and missing energy. The observation of these signals would rely on two crucial detector performance parameters, namely a very good  $p_T^{\text{miss}}$  resolution and a very good  $\tau$  jet identification with excellent rejection of non  $\tau$  jets. The former performance parameter is necessary for the reconstruction of the  $\tau\mu$  invariant mass in  $A^0/H^0 \rightarrow \tau^\pm\mu^\mp$  (as demonstrated in the above analysis) and also for the  $\tau\tau$  invariant mass in  $A^0/H^0 \rightarrow \tau^+\tau^-$  [50, 51] while the latter performance parameter allows for the suppression of various backgrounds containing fake  $\tau$  jets. We show in this section that the reconstruction procedures presented in this paper for  $A^0/H^0 \rightarrow \tau\mu$  and described in [50, 51] for  $A^0/H^0 \rightarrow \tau\tau$  allow for the identification of each of these processes although their final states are similar.

TABLE V: The efficiencies (in percent) of the cuts used in the current analysis. The first three cuts are effective in reducing the dominant  $W^\pm$ +jets events while the other cuts suppress the rest of the backgrounds efficiently.

Cut	$A^0/H^0 \rightarrow \tau^\pm\mu^\mp$					$t\bar{t}$	$W^\pm Z^0$	$W^+W^-$	$Z^0(\gamma^*)$	$W^\pm$ +jets
	120	130	140	150	160 GeV					
(1)	16.3	17.0	16.9	17.2	20.9	$3.0 \cdot 10^{-1}$	7.2	16.3	0.2	0.5
(2)	9.1	9.6	9.7	9.9	12.1	$1.5 \cdot 10^{-2}$	0.50	1.3	0.09	$2.2 \cdot 10^{-2}$
(3)	4.4	4.8	4.6	4.9	5.9	$0.7 \cdot 10^{-2}$	0.25	0.65	0.04	$2.2 \cdot 10^{-2}$
(4)	2.7	3.0	2.9	3.1	3.8	$2.7 \cdot 10^{-3}$	0.10	0.40	0.02	$1.9 \cdot 10^{-3}$
(5)	2.4	2.7	2.6	2.8	3.5	$2.4 \cdot 10^{-3}$	0.10	0.40	0.01	$1.1 \cdot 10^{-3}$
(6)	1.7	2.1	2.2	2.5	3.2	$2.2 \cdot 10^{-3}$	0.05	0.20	$2.4 \cdot 10^{-4}$	$5.3 \cdot 10^{-4}$
(7)	1.2	2.0	2.2	2.5	3.1	$2.1 \cdot 10^{-3}$	0.05	0.20	$1.6 \cdot 10^{-4}$	$4.3 \cdot 10^{-4}$

## 2. Optimization for $A^0/H^0 \rightarrow \tau\tau$

It is also important to show that the analysis technique optimized for the search for the  $A^0/H^0 \rightarrow \tau\tau$  signal is capable of separating the  $\tau\tau$  final state from the  $\tau\mu$  events. We have therefore examined  $A^0/H^0 \rightarrow \tau\mu$  events according to the  $A^0/H^0 \rightarrow \tau\tau$  analysis technique which we recall succinctly as follows [50, 51]:

- One isolated  $\mu$  with  $p_T > 24$  GeV and  $|\eta| < 2.5$ , one hadronic  $\tau$  jet with  $E_T^{jet} > 40$  and  $|\eta| > 2.5$  and b-jet veto.
- $E_T^{miss} > 18$  GeV.
- The transverse mass  $m_T(\text{lepton}-E_T^{miss}) < 25$  GeV.
- $1.8 < \Delta\phi < 2.9$  rad or  $3.4 < \Delta\phi < 4.9$  rad, where  $\Delta\phi$  is the azimuthal opening angle between the  $\tau$  jet and the isolated  $\mu$ . This cut is needed for the reconstruction of the  $\tau\tau$  invariant mass  $m_{\tau\tau}$ . Indeed, the invariant mass  $m_{\tau\tau}$  of the pair of  $\tau$  leptons produced in the process

$$A^0/H^0 \rightarrow \tau\tau \rightarrow \text{jet } \nu_\tau \mu \nu_\mu \nu_\tau$$

can be reconstructed assuming that  $m_\tau = 0$ , that the  $\tau$  detected products (in this case the  $\tau$  jet and the  $\mu$ ) are not back-to-back, and also that the direction of the neutrino system from each  $\tau$  decay coincides with that of the detected product:

$$m_{\tau\tau} = \sqrt{2(E_1 + E_{\nu 1})(E_2 + E_{\nu 2})(1 - \cos\theta)}. \quad (32)$$

$E_1$  and  $E_2$  are the visible energies from the  $\tau$  decays,  $\theta$  is the angle between the directions of the detected products, and  $E_{\nu 1}$  and  $E_{\nu 2}$  are the energies of the two neutrino systems, obtained by solving the system of equations

$$p_x^{miss}(p_y^{miss}) = [E_{\nu 1}\bar{u}_1]_{x(y)} + [E_{\nu 2}\bar{u}_2]_{x(y)},$$

where  $\bar{u}_1$  and  $\bar{u}_2$  are the directions of the detected products, and  $p_x^{miss}$  and  $p_y^{miss}$  the components of the  $E_T^{miss}$  vector. The above system of equations can be solved if the determinant, which is proportional to  $\sin\Delta\phi$ , is not zero. Further details of

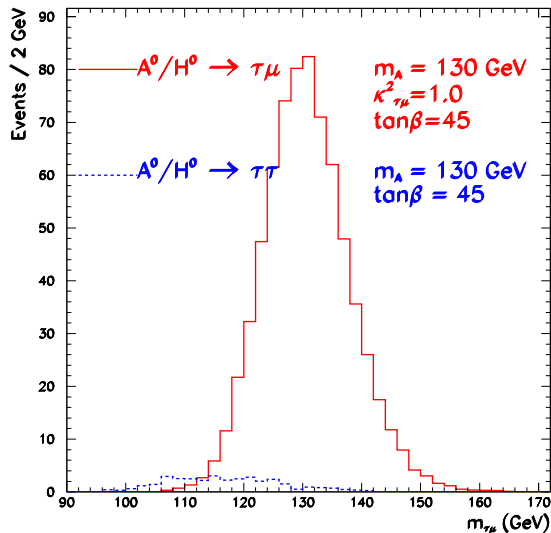


FIG. 13: The reconstructed  $m_{\tau\mu}$  invariant mass for  $A^0/H^0 \rightarrow \tau\mu$  and  $A^0/H^0 \rightarrow \tau^+\tau^-$   $m_A = 130$  GeV and  $\kappa_{\tau\mu} = 1$  ( $\tan\beta = 45$ ,  $\alpha = -0.58$  rad), i.e. set 2 of Table I using the analysis procedure presented above. The existence of the  $A^0/H^0 \rightarrow \tau^+\tau^-$  signal would constitute an additional background for the  $A^0/H^0 \rightarrow \tau^\pm\mu^\mp$  process.

## 1. Optimization for $A^0/H^0 \rightarrow \tau\mu$

We generated  $A^0/H^0 \rightarrow \tau\tau$  events and analyzed them according to the analysis procedure described in section IV A. The relative efficiencies of the cuts described in section IV A for  $A^0/H^0 \rightarrow \tau\mu$  and  $A^0/H^0 \rightarrow \tau\tau$  final states are shown in Table VI. From Figure 13, we see that at the same Higgs boson mass, the reconstructed  $\tau\mu$  invariant mass for the  $A^0/H^0 \rightarrow \tau^+\tau^-$  events peaks at lower values.

TABLE VI: The relative efficiencies (in percent) of the cuts used in the current analysis for  $A^0/H^0 \rightarrow \tau\tau$  events, to be compared to Table V where the efficiencies for  $A^0/H^0 \rightarrow \tau\mu$  are shown.

Cut	$A^0/H^0 \rightarrow \tau\tau$				
	120	130	140	150	160 GeV
(1)	2.0	4.2	2.1	1.95	1.77
(2)	0.6	1.1	0.6	0.52	0.47
(3)	0.3	0.6	0.3	0.26	0.23
(4)	0.1	0.24	0.12	0.11	0.10
(5)	0.09	0.18	0.09	0.08	0.08
(6)	0.01	0.04	0.02	0.03	0.03
(7)	$0.8 \cdot 10^{-2}$	0.02	0.02	0.02	0.03

TABLE VII: The relative efficiencies (in percent) of the cuts used in the search for  $A^0/H^0 \rightarrow \tau\tau$  [50, 51] and re-stated briefly in the text ( $m_A = 130$  GeV).

Cut	$A^0/H^0 \rightarrow \tau^\pm\mu^\mp$	$A^0/H^0 \rightarrow \tau\tau$
(a)	15.1	3.1
(b)	5.3	1.9
(c)	0.2	1.5
(d)	0.02	0.3

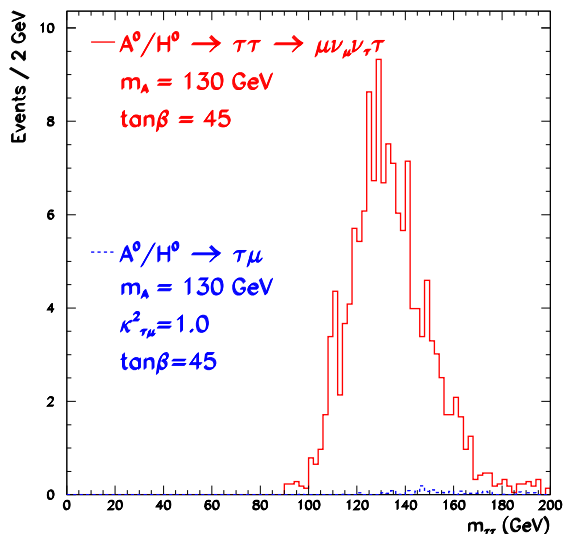


FIG. 14: The reconstructed  $m_{\tau\tau}$  invariant mass for  $A^0/H^0 \rightarrow \tau\tau$  and  $A^0/H^0 \rightarrow \tau\mu$ , for  $m_A = 130$  GeV and  $\kappa_{\tau\mu} = 1$  ( $\tan\beta = 45$ ,  $\alpha = -0.58$  rad), i.e. set 2 of Table I using the analysis procedure presented in [50, 51]. The existence of the  $A^0/H^0 \rightarrow \tau\mu$  signal would constitute a negligible background for the  $A^0/H^0 \rightarrow \tau\tau$  process.

the  $m_{\tau\tau}$  reconstruction are well documented elsewhere [50, 51].

The relative efficiencies of the cuts (a)–(d) for the  $\tau\mu$  and  $\tau\tau$  final states are shown in Table VII. Figure 14

shows the reconstructed  $m_{\tau\tau}$  invariant mass distribution for both final states. The  $\tau\mu$  events would contribute a negligible background under the  $\tau\tau$  signal.

The reconstruction procedure for  $A^0/H^0 \rightarrow \tau^+\tau^-$  described in [50, 51] and the analysis steps presented above for  $A^0/H^0 \rightarrow \tau^\pm\mu^\mp$ , would allow for the separation of both signals, with each contributing a small residual background under peak of the other as shown in Figures 13 and 14.

### C. Leptonic $\tau$ decay

Thus far, we have considered the hadronic final state of the  $\tau$  lepton, and the major irreducible background comes from  $W$ +jets events where a jet is mis-identified as a hadronic  $\tau$  jet. Indeed, the residual SM background shown in Figure 12 is dominated by  $W$ +jets events whose rate is several orders of magnitude higher than the signal rates as shown in Table IV. In this section, we examine the leptonic decay of the  $\tau$ , namely  $\tau \rightarrow e\nu_e\bar{\nu}_\tau$ . Although the branching fraction of  $\tau \rightarrow e\nu_e\bar{\nu}_\tau$  is only  $\sim 18\%$  compared to  $65\%$  for  $\tau \rightarrow (jet)\nu_\tau$ , the identification of the electron is easier with an efficiency of  $90\%$  whereas the  $\tau$  jet identification efficiency is much lower: in the above analysis, we assume a  $\tau$  jet identification efficiency of  $30\%$ , corresponding to a jet rejection factor of  $\sim 400$  — see [50] for details. Furthermore, the leptonic decay of the  $\tau$  will not be sensitive to the  $W$ +jets background. We search for a signal final state containing two isolated leptons, one electron and the other a  $\mu$  with no hadronic activity. The major SM backgrounds in this case are shown in Table IV — processes listed in (25) — except

TABLE VIII: The rates,  $\sigma \times \text{BR}(\text{pb})$ , for the signal  $gg \rightarrow A^0/H^0 \rightarrow \tau^+\mu^- + \tau^-\mu^+$ , and the backgrounds at the TeVatron. We assume  $\kappa_{\tau\mu} = 1$  and  $\tan\beta = 45$ .

Process	$m_A$ (GeV)	$m_H$ (GeV)	$\sigma \times \text{BR}(\text{pb})$
$gg \rightarrow A^0/H^0 \rightarrow \tau^+\mu^- + \tau^-\mu^+$	119.3	128.4	$1.41 \cdot 10^{-1}$
	129.3	130.1	$0.79 \cdot 10^{-1}$
	139.2	140.2	$0.33 \cdot 10^{-1}$
	149.1	150.0	$0.11 \cdot 10^{-1}$
	159.1	160.0	$0.15 \cdot 10^{-2}$
$gg \rightarrow A^0/H^0 \rightarrow \tau\tau$	119.3	128.4	3.90
	129.3	130.1	2.84
	139.2	140.2	1.79
	149.1	150.0	1.16
	159.1	160.0	0.75
$p\bar{p} \rightarrow Z^0(\gamma^*) \rightarrow \tau^+\tau^- \rightarrow \mu^+\nu_\mu\bar{\nu}_\tau\tau^-$		$3.24 \cdot 10^3$	
$p\bar{p} \rightarrow W^\pm + \text{jets} \rightarrow \mu^\pm\nu_\mu + \text{jets}$		$3.21 \cdot 10^3$	

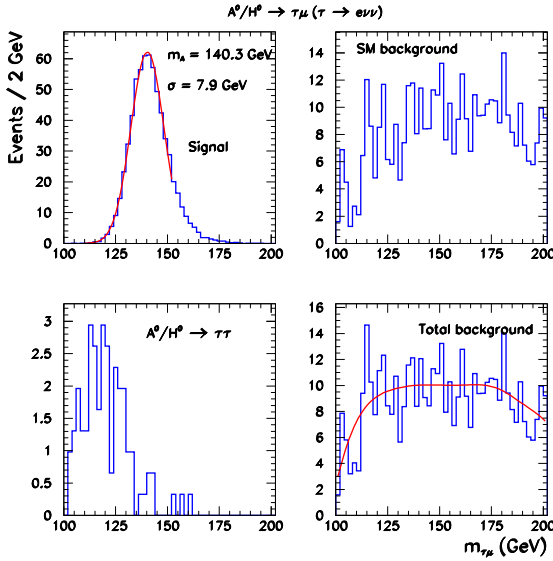


FIG. 15: The reconstructed invariant mass  $m_{\tau\mu}$  in the leptonic decay of the  $\tau$  ( $\rightarrow e\nu\nu$ ) for the signal ( $m_A = 140$  GeV,  $\tan\beta = 45$ ,  $\kappa = 1$ ), the SM backgrounds and the  $A^0/H^0 \rightarrow \tau\tau$  background.

for the  $W$ +jets background, in addition to:

$$\begin{aligned} t\bar{t} &\rightarrow \mu\nu_\mu b e \nu_e \bar{b}, \\ WW &\rightarrow \mu\nu_\mu e \nu_e. \end{aligned} \quad (33)$$

The reconstruction of the signal is exactly as described in section IV A, except for the cuts (2) and (3) which were implemented for the suppression of the  $W$ +jets events and for the selection of the one prong hadronic  $\tau$  decays. These cuts are no longer necessary and are not used in the search for the leptonic decay of the  $\tau$ . Figure 15 shows the reconstructed  $\tau\mu$  invariant mass for the signal  $A^0/H^0 \rightarrow \tau\mu$ , the SM backgrounds and for the  $A^0/H^0 \rightarrow \tau\tau$  background with one  $\tau$  decaying to lep-

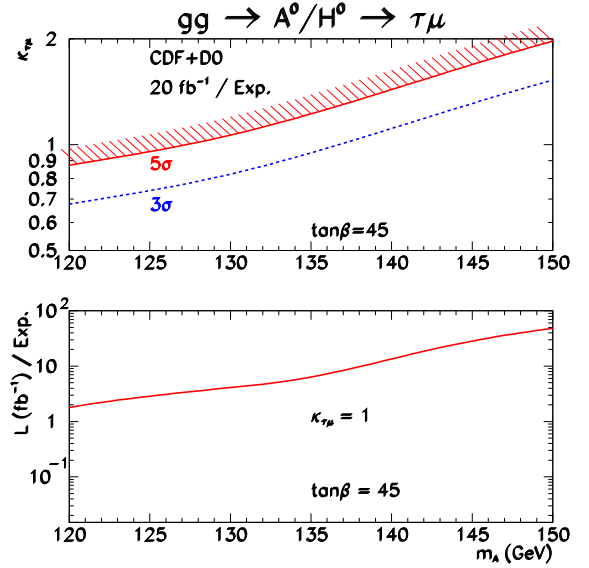


FIG. 16: The discovery reach at the TeVatron in the combined  $\tau \rightarrow \text{jet}\nu_\tau$  and  $\tau \rightarrow e\nu_e\nu_\tau$  channels. The signal would yield a  $5\sigma$  significance for  $0.87 \lesssim \kappa_{\tau\mu} \lesssim 2.0$  and for a Higgs boson mass  $120 \lesssim m_A \lesssim 150$  GeV. The luminosity needed for a 95% confidence level exclusion is shown in the bottom plot.

tons:  $\tau \rightarrow e\nu\nu$ . In this channel too, the signal can be observed with significances exceeding  $5\sigma$  depending on the LFV coupling parameter  $\kappa_{\tau\mu}$ .

#### D. Prospects at the TeVatron

Table VIII shows the estimated signal and background rates at the TeVatron where we propose to search for  $A^0/H^0 \rightarrow \tau^\pm\mu^\mp$  with the neutral Higgs bosons of the 2HDM produced through gluon fusion:  $gg \rightarrow A^0/H^0$ . The signal-to-background ratios and the signal signifi-

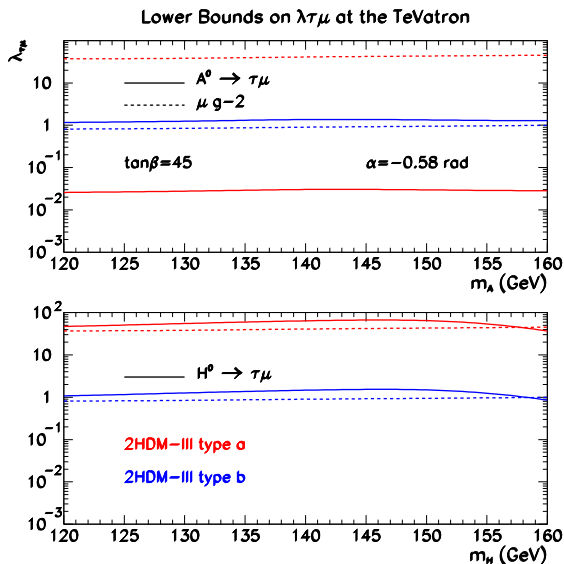


FIG. 17: The achievable lower bounds on the LHV coupling  $\lambda_{\tau\mu}$  at the TeVatron (CDF + DØ) obtained from the summed signal in the hadronic and leptonic decays of the  $\tau$  lepton. To obtain these bounds, we use the values of  $\kappa_{\tau\mu}$  at  $5\sigma$  shown in Figure 16 —  $20 \text{ fb}^{-1}$  per experiment. The current bounds on  $\lambda_{\tau\mu}$  obtained from the muon  $g-2$  data are also shown. For the muon  $g-2$  data, the curves at higher  $\lambda_{\tau\mu}$  values correspond to the 2HDM-III type a and the lower curves to the 2HDM-III type b. This trend is the same for  $H^0 \rightarrow \tau\mu$  (bottom plot) but it is reversed for  $A^0 \rightarrow \tau\mu$  (top plot).

cances calculated within  $\pm 2\sigma$  of the reconstructed Higgs mass peak, for an integrated luminosity of  $20 \text{ fb}^{-1}$  per experiment, are shown in Table IX for  $\kappa_{\tau\mu}^2 = 1$  and  $\tan\beta = 45$ . At the TeVatron, a significant signal ( $> 5\sigma$ ) can be detected for Higgs boson masses around 120 GeV and high  $\tan\beta$  ( $\sim 45$ ), assuming  $\kappa_{\tau\mu} \sim 1$ . We show in Figure 16 the discovery reach at the TeVatron and the luminosity required for a 95% confidence level exclusion for large  $\tan\beta$ . For low  $\tan\beta$  values ( $\lesssim 10$ ), the signal production rate decreases by more than an order of magnitude compared to the case shown in Table VIII so that the detection of this process at the TeVatron would require very large values of the LFV coupling  $\lambda_{\tau\mu}$ . However, one would expect the LFV couplings  $\lambda_{ij} \sim \mathcal{O}(1)$  [35, 48] — see Equations (23) and (24). Therefore, at the TeVatron, this channel would be viable only in the event of a large  $\tan\beta$  value and for  $\kappa_{\tau\mu} \sim 1$  — see Table III for the correspondence between  $\kappa_{\tau\mu}$  and  $\lambda_{\tau\mu}$ . Figure 17 shows the corresponding expected limits on  $\lambda_{\tau\mu}$  at the TeVatron: the reach in  $\lambda_{\tau\mu}$  would be extended, at large  $\tan\beta$ , beyond that obtained from the muon  $g-2$  experiment, for  $A^0 \rightarrow \tau\mu$  in the 2HDM-III type a.

As shown in Figure 17, the bounds on  $\lambda_{\tau\mu}$  would be different for the Higgs bosons  $A^0$ ,  $H^0$  and  $h^0$  because of

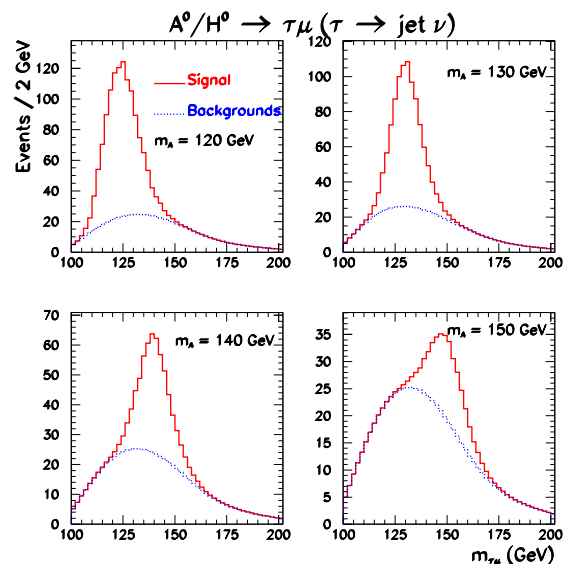


FIG. 18: The reconstructed invariant mass  $m_{\tau\mu}$ , after cut (7), of the signal plus the backgrounds in the hadronic  $\tau$  decay channel for  $m_A = 120, 130, 140$  and  $150$  GeV, and for an integrated luminosity of  $30 \text{ fb}^{-1}$  at the LHC. For the assumed value of the LFV coupling parameter ( $\kappa_{\tau\mu}^2 = 1$ ), the signal can be observed with a significance exceeding  $5\sigma$  up to  $m_A = 150$  GeV.

their different LFV Yukawa couplings — see sections II-III and the appendix.

### E. Prospects at the LHC

The signal and background rates at the LHC are shown in Table IV. In Figures 18 and 19, we show the reconstructed  $m_{\tau\mu}$  invariant mass for several values of the Higgs mass, and for an integrated luminosity of  $30 \text{ fb}^{-1}$ , and for the LFV coupling parameter  $\kappa_{\tau\mu}^2 = 1$ .

The signal-to-background ratios and the signal significances are calculated with the events reconstructed within  $\pm 2\sigma$  of the reconstructed Higgs mass. As shown in Table X, a significant signal can be observed at the LHC for Higgs masses in the range 120 to 150 GeV for the LFV coupling parameter  $\kappa_{\tau\mu} \sim \mathcal{O}(1)$ . Around 160 GeV, as the  $H_{SM}^0 \rightarrow W^+W^-$  channel opens up, the rate for  $A^0/H^0 \rightarrow \tau^\pm\mu^\mp$  decreases so drastically that the observation of a significant signal would be possible only in the event of  $\kappa_{\tau\mu} > 1$ .

The constraints on this LFV coupling  $\lambda_{\tau\mu}$  from low energy experiments are rather weak — see the discussion in section II on low energy bounds. From Equation (22), the signal rate scales like  $\kappa_{\tau\mu}^2$  and we show in Figure 20 the value of  $\kappa_{\tau\mu}$  at which the signal yield a  $5\sigma$  significance around the Higgs boson mass peak. The LFV coupling  $0.18 \lesssim \kappa_{\tau\mu} \lesssim 1.0$  can be reached at the LHC,

TABLE IX: The expected signal-to-background ratios and signal significances ( $\tau \rightarrow \text{jet } \nu/\tau \rightarrow e\nu\nu$ ) for two experiments at the TeVatron, assuming  $\kappa_{\tau\mu}^2 = 1$  and 5% systematic uncertainty on the background shape and normalization.

$m_A$ (GeV) $\rightarrow$	120	130	140	150
Signal ( $S$ )	10/29	7/19	3/13	1/5
Backgrounds ( $B$ )	4/42	4/44	3/51	2/62
$S/B$	2.4/0.7	1.8/0.4	1.0/0.3	0.5/0.1
$S/\sqrt{B}$	5.0/4.3	3.5/2.7	1.7/1.7	1.2/0.6
Combined $S/\sqrt{B}$	6.6	4.4	2.4	1.3

TABLE X: The signal-to-background ratios and signal significances calculated within  $\pm 2\sigma$  of the reconstructed Higgs mass  $\langle m_A \rangle$  for  $\tau \rightarrow \text{jet } \nu/\tau \rightarrow e\nu\nu$  — one experiment at the LHC — with an integrated luminosity of  $30 \text{ fb}^{-1}$ , assuming  $\kappa_{\tau\mu}^2 = 1$  and 5% systematic uncertainty from the residual background shape and normalization.

$m_A$ (GeV) $\rightarrow$	120	130	140	150	160
$\langle m_A \rangle$ (GeV)	124.6/125.2	130.0/130.7	139.9/140.6	149.7/150.0	159.4/159.8
$\sigma$ (GeV)	7.5/7.3	7.0/7.0	7.6/8.2	8.1/9.1	8.4/10.4
Signal ( $S$ )	943/1142	687/816	349/624	144/279	23/57
Backgrounds ( $B$ )	360/134	397/140	376/163	296/198	223/226
$S/B$	2.6/8.5	1.7/5.8	0.9/3.8	0.5/1.4	0.1/0.3
$S/\sqrt{B}$	36.1/85.4	24.4/59.4	12.9/41.2	6.3/16.2	1.2/3.0
Combined $S/\sqrt{B}$	92.7	64.2	43.2	17.4	3.2

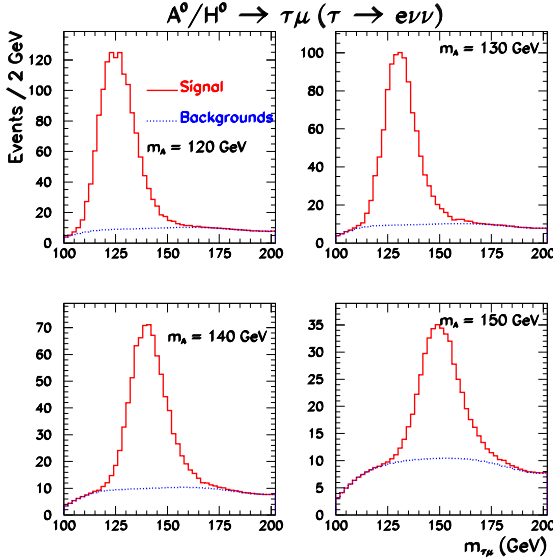


FIG. 19: The same as Figure 18 but with the leptonic decay of the  $\tau$  ( $\rightarrow e\nu_e\nu_\tau$ ).

combining ATLAS and CMS data for Higgs boson masses  $120 \lesssim m_A \lesssim 160 \text{ GeV}$ . Figure 20 also shows in the bottom plot, the luminosity needed at the LHC to achieve a  $2\sigma$  (95% CL) exclusion. At the LHC, assuming the LFV coupling parameter  $\kappa_{\tau\mu} \sim \mathcal{O}(1)$ , few years of low luminosity data would be enough to exclude this model in mass range  $120 < m_A < 150 \text{ GeV}$  and at low  $\tan\beta$ .

For high  $\tan\beta$  values, a 95% CL exclusion can be established in one year of data taking or less for the mass range considered. In Figure 21, we show the expected bounds on  $\lambda_{\tau\mu}$  at the LHC using the values of  $\kappa_{\tau\mu}$  at  $5\sigma$  from Figure 20 and we see that the reach in  $\lambda_{\tau\mu}$  would be extended beyond the muon  $g-2$  limits.

## V. CONCLUSIONS

In models with several Higgs doublets, FCNC and LFV couplings exist at tree level because the diagonalization of the up-type and the down-type mass matrices does not ensure the diagonalization of the Higgs-fermion coupling matrices. In the 2HDM-I and II, a discrete symmetry suppresses FCNC and LFV couplings at tree level by restricting fermions of a given electric charge to couple to at most one Higgs doublet. In the 2HDM-III, no discrete symmetry is invoked and the flavor changing couplings are parameterized in terms of the fermion mass hierarchy to be in agreement with the severe experimental constraints on FCNC and LFV couplings with the first generation index. The arbitrariness of the FCNC and LFV couplings of the second and the third generations can be constrained in low energy and collider experiments. The deviation of the measured muon anomalous magnetic moment from the SM prediction offers weak bounds on the LFV coupling parameter  $\lambda_{\tau\mu}$ .

We have investigated the achievable bound on  $\kappa_{\tau\mu}$  and  $\lambda_{\tau\mu}$  at hadron colliders by studying the  $gg \rightarrow A^0/H^0 \rightarrow \tau^\pm \mu^\mp$  signal observability.

Considering the hadronic decay of the  $\tau$  lepton, the

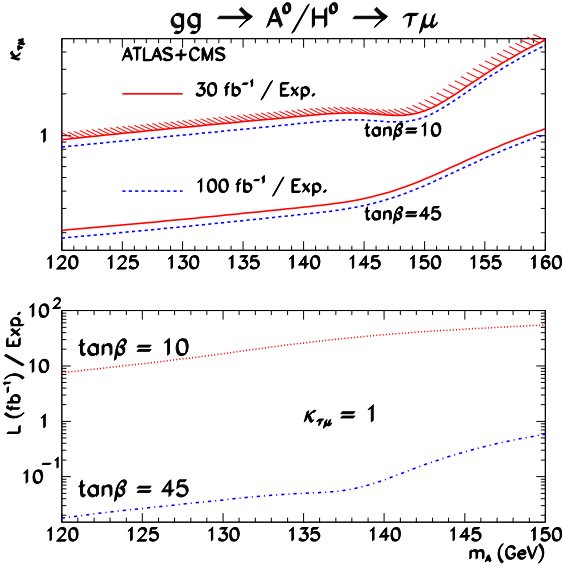


FIG. 20: The  $5\sigma$  discovery reach in the  $(m_A, \kappa_{\tau\mu})$  plane, using the combined  $\tau \rightarrow \text{jet } \nu_\tau$  and  $\tau \rightarrow e\nu_e\nu_\tau$  signals, for ATLAS + CMS (top plot). The  $A^0/H^0 \rightarrow \tau^\pm\mu^\mp$  signal would yield a  $5\sigma$  significance for  $0.18 \lesssim \kappa_{\tau\mu} \lesssim 1.0$  and for a Higgs boson mass  $120 \lesssim m_A \lesssim 160$  GeV. The bottom plot shows the luminosity needed for a 95% confidence level exclusion as a function of  $m_A$  for low and high  $\tan\beta$  assuming  $\kappa_{\tau\mu} = 1$ .

main backgrounds of this process are  $Z^0(\gamma) \rightarrow \tau^+\tau^-$  and  $W^\pm + \text{jets}$  events where  $W^\pm \rightarrow \mu^\pm\nu_\mu$  and a jet is mis-identified as a  $\tau$  jet. We search for an isolated  $\mu$  and one  $\tau$  jet, and we applied a jet veto and a b-jet veto to reject multi-jet final states from  $t\bar{t}$  and  $W^\pm + \text{jets}$ . Further reduction of the backgrounds is achieved by exploiting the differences in the event topology of the signal and the various backgrounds. Although the background rates are several orders of magnitude higher than the signal rate, three main detector performance parameters have been crucial in extracting a significant signal: a good  $\tau$  jet identification and rejection against non  $\tau$  jets, the tracking capability for the identification of the charged tracks in one prong hadronic  $\tau$  decays, and the missing momentum resolution.

We also investigated the leptonic decay of the  $\tau$  ( $\rightarrow e\nu\nu$ ) where the  $W + \text{jets}$  event do not contribute a significant background. In this case, we require a final state containing one isolated  $\mu$ , one isolated electron, and we use jet veto and b-jet veto to suppress the  $t\bar{t}$  background. The leptonic decay of the  $\tau$  gives a better sensitivity. The signal significances are estimated based on expected events in both the hadronic and the leptonic  $\tau$  decay channels.

The analysis steps described above reconstruct the  $\tau\mu$  invariant mass to within  $\sim 1$  GeV of the Higgs boson mass (except at  $m_A = 120$  GeV where the  $A^0$  and the  $H^0$  bosons are not degenerate and the summed signal peaks

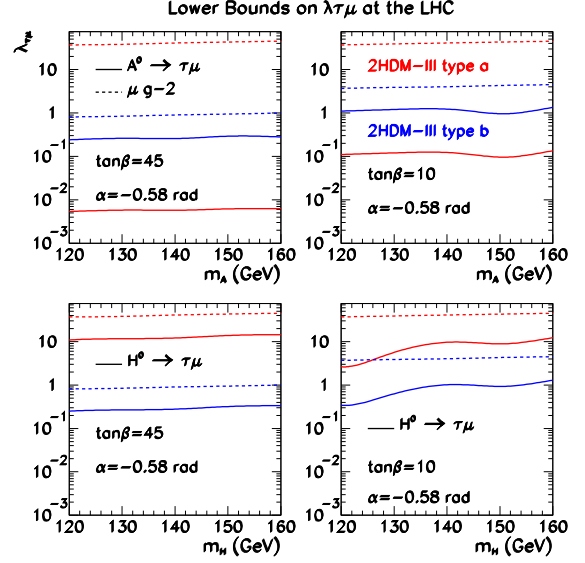


FIG. 21: The achievable bounds on the LHV coupling  $\lambda_{\tau\mu}$  at the LHC (ATLAS + CMS) from the combined hadronic and leptonic  $\tau$  decay channels —  $100 \text{ fb}^{-1}$  per experiment. For low or high  $\tan\beta$ , the lower bounds on  $\lambda_{\tau\mu}$  at the LHC would be extended beyond that of the muon  $g-2$  experiment. For the muon  $g-2$  data, the curves at higher  $\lambda_{\tau\mu}$  values correspond to the 2HDM-III type a and the lower curves to the 2HDM-III type b. This trend is the same for  $H^0 \rightarrow \tau\mu$  (bottom plots) but it is reversed for  $A^0 \rightarrow \tau\mu$  (top plots).

somewhere in the middle as a result), and also differentiate the  $A^0/H^0 \rightarrow \tau^+\tau^-$  events from the  $A^0/H^0 \rightarrow \tau^\pm\mu^\mp$  signal.

With an integrated luminosity of  $20 \text{ fb}^{-1}$  at the Tevatron, a signal for  $0.87 \lesssim \kappa_{\tau\mu} \lesssim 2.0$  could be detected with a significance of  $5\sigma$  for Higgs boson masses  $120 \lesssim m_A \lesssim 150$  GeV, corresponding to a reach in  $\lambda_{\tau\mu}$  of the order  $0.03/1.0$  for the 2HDM-III type a/type b. In case the signal is not observed and assuming  $\kappa_{\tau\mu} \sim \mathcal{O}(1)$ , a 95% CL exclusion can be set with  $< 14 \text{ fb}^{-1}$  of data for  $120 \lesssim m_A \lesssim 140$  GeV.

The sensitivity will be improved at the LHC where  $\kappa_{\tau\mu} \sim 0.18$  could be reached with  $100 \text{ fb}^{-1}$  — this would correspond to a lower bound in  $\lambda_{\tau\mu} \sim 0.01/0.1$  for the 2HDM-III type a/type b. A 95% CL exclusion could be set after just a few years of running at low luminosity if the signal is not observed.

At the LHC, the reach in the LFV coupling  $\lambda_{\tau\mu}$  would be extended beyond that expected at the Tevatron and also beyond that obtained from the muon  $g-2$  data: a factor of 10 to 100 better depending on  $\tan\beta$  and  $\alpha$ .

### Acknowledgments

This work is partially performed within the ATLAS collaboration and we thank collaboration members for helpful comments. We have used the physics analysis framework and tools which are the results of collaboration wide efforts. The authors would like to thank E. Richter-Was and G. Azuelos for discussions and comments, and also to T. Sjöstrand for helpful correspondence.

### Appendix

In this appendix we give the Lagrangian of the lepton flavor conserving and violating Yukawa couplings of the 2HDM type III using the results of [52] with the addition of the charged Higgs part. The leptonic Yukawa Lagrangian reads:

$$-\mathcal{L} = \eta_{ij} \bar{l}_{iL}^0 \varphi_1 l_{jR}^0 + \xi_{ij} \bar{l}_{iL}^0 \varphi_2 l_{jR}^0 + \text{h.c.} \quad (34)$$

where  $\varphi_{1,2}$  are the two Higgs doublets

$$\varphi_1 = \begin{pmatrix} \phi_1^+ \\ \phi_1^0 \end{pmatrix} \quad \varphi_2 = \begin{pmatrix} \phi_2^+ \\ \phi_2^0 \end{pmatrix} \quad (35)$$

with vacuum expectation values

$$\langle \varphi_1 \rangle_0 = \frac{1}{\sqrt{2}} \begin{pmatrix} 0 \\ v_1 \end{pmatrix} \quad \langle \varphi_2 \rangle_0 = \frac{1}{\sqrt{2}} \begin{pmatrix} 0 \\ v_2 e^{i\theta} \end{pmatrix}, \quad (36)$$

where in the following we set  $\theta = 0$  and therefore we consider a CP conserving Higgs sector. The parameters  $\eta_{ij}$  and  $\xi_{ij}$  are non diagonal  $3 \times 3$  matrices and  $i, j$  are family indices. The neutral and charged mass eigenstates

are related to the states of (35) by

$$\begin{pmatrix} \cos \beta & -\sin \beta \\ \sin \beta & \cos \beta \end{pmatrix} \begin{pmatrix} G_W^\pm \\ H^\pm \end{pmatrix} = \begin{pmatrix} \phi_1^\pm \\ \phi_2^\pm \end{pmatrix} \\ \begin{pmatrix} \cos \beta & -\sin \beta \\ \sin \beta & \cos \beta \end{pmatrix} \begin{pmatrix} G_Z^0 \\ A^0 \end{pmatrix} = \sqrt{2} \begin{pmatrix} \Im \phi_1^0 \\ \Im \phi_2^0 \end{pmatrix} \quad (37) \\ \begin{pmatrix} \cos \alpha & -\sin \alpha \\ \sin \alpha & \cos \alpha \end{pmatrix} \begin{pmatrix} H^0 \\ h^0 \end{pmatrix} = \sqrt{2} \begin{pmatrix} \Re \phi_1^0 - v_1/\sqrt{2} \\ \Re \phi_2^0 - v_2/\sqrt{2} \end{pmatrix}$$

where  $\Re \phi$  and  $\Im \phi$  are the real and imaginary parts of the complex scalar fields  $\phi$ ,  $\tan \beta = v_2/v_1$ ,  $\alpha$  is the CP-even neutral Higgs sector mixing angle,  $G_Z^0$  and  $G_W^\pm$  are the would-be Goldstone bosons of  $Z$  and  $W$  vector bosons, and  $H^\pm$ ,  $A^0$ ,  $H^0$ ,  $h^0$  are the physical Higgs bosons of the 2HDM. The Lagrangian (34) in terms of the mass eigenstates is obtained by a unitary transformation

$$l_{L,R} = V_{L,R} l_{L,R}^0 \quad (38)$$

and one can write the diagonal mass matrix for the three leptons

$$M_l^{\text{diag}} = V_L \left( \frac{v_1}{\sqrt{2}} \eta + \frac{v_2}{\sqrt{2}} \xi \right) V_R^\dagger \quad (39)$$

and either solve for  $\xi$  (rotation of type a)

$$\xi = \frac{\sqrt{2}}{v_2} V_L^\dagger M_l^{\text{diag}} V_R - \frac{v_1}{v_2} \eta \quad (40)$$

or for  $\eta$  (rotation of type b)

$$\eta = \frac{\sqrt{2}}{v_1} V_L^\dagger M_l^{\text{diag}} V_R - \frac{v_2}{v_1} \xi. \quad (41)$$

In terms of  $\eta$  the leptonic Lagrangian reads (type a):

---


$$\mathcal{L}^a = -\frac{m_i}{v \sin \beta} \bar{l}_i l_i (\cos \alpha h^0 + \sin \alpha H^0) - i \frac{m_i \cot \beta}{v} \bar{l}_i \gamma_5 l_i A^0 - \frac{m_i \cot \beta}{\sqrt{2} v} \bar{n}_i (1 + \gamma_5) l_i H^+ \\ + \frac{1}{\sqrt{2} \sin \beta} \bar{l}_i \eta_{ij} l_j [\cos(\alpha - \beta) h^0 + \sin(\alpha - \beta) H^0] + \frac{i}{\sqrt{2} \sin \beta} \bar{l}_i \eta_{ij} \gamma_5 l_j A^0 + \frac{1}{2 \sin \beta} \bar{n}_i \eta_{ij} (1 + \gamma_5) l_j H^+ + \text{h.c.} \quad (42)$$

while in terms of  $\xi$  the leptonic Lagrangian reads (type b):

$$\mathcal{L}^b = -\frac{m_i}{v \cos \beta} \bar{l}_i l_i (\sin \alpha h^0 - \cos \alpha H^0) + i \frac{m_i \tan \beta}{v} \bar{l}_i \gamma_5 l_i A^0 + \frac{m_i \tan \beta}{\sqrt{2} v} \bar{n}_i (1 + \gamma_5) l_i H^+ \\ - \frac{1}{\sqrt{2} \cos \beta} \bar{l}_i \xi_{ij} l_j [\cos(\alpha - \beta) h^0 + \sin(\alpha - \beta) H^0] - \frac{i}{\sqrt{2} \cos \beta} \bar{l}_i \xi_{ij} \gamma_5 l_j A^0 - \frac{1}{2 \cos \beta} \bar{n}_i \xi_{ij} (1 + \gamma_5) l_j H^+ + \text{h.c.} \quad (43)$$


---

where  $n$  is the neutrino field,  $v = (\sqrt{2} G_F)^{-1/2} = 246$  GeV is the SM vacuum expectation value, related

to  $v_1$  and  $v_2$  by

$$v = \sqrt{v_1^2 + v_2^2}. \quad (44)$$



Note that the Lagrangian (42) corresponds in the lepton flavor conserving part to 2HDM-I, while the Lagrangian (43) to 2HDM-II.

The couplings for lepton flavor conserving and violating Yukawa interactions  $h_{ij}$  can be read directly from the Lagrangian (42) and (43). As an example the lepton flavor conserving charged Higgs coupling squared from (43) (which is the same as in 2HDM-II) is

$$h_{\mu\nu}^2 = \frac{m_\mu^2 \tan^2 \beta}{2v^2} = \frac{G_F m_\mu^2 \tan^2 \beta}{\sqrt{2}} \quad (45)$$

$$\Gamma(H^0 \rightarrow l_i^+ l_j^-) = m_H \frac{N_c \lambda_{ij}^2}{8\pi} \frac{m_i m_j}{v^2} \theta^2(\alpha, \beta) \left(1 - \frac{(m_i + m_j)^2}{m_H^2}\right)^{3/2} \left(1 - \frac{(m_i - m_j)^2}{m_H^2}\right)^{1/2}, \quad (46)$$

$$\Gamma(A^0 \rightarrow l_i^+ l_j^-) = m_A \frac{N_c \lambda_{ij}^2}{8\pi} \frac{m_i m_j}{v^2} \theta^2(\alpha, \beta) \left(1 - \frac{(m_i + m_j)^2}{m_A^2}\right)^{1/2} \left(1 - \frac{(m_i - m_j)^2}{m_A^2}\right)^{3/2}, \quad (47)$$

where  $N_c = 3$  for quarks and  $N_c = 1$  for leptons. For a flavor conserving decay  $\lambda_{ii} = 1$  and  $m_i = m_j$ .  $\theta(\alpha, \beta)$  is a function of the mixing parameters, given in Table XI. The Higgs couplings to gauge bosons follow from gauge

in agreement with the erratum in [1] (see the discussion there for a comment on other results in the literature).

We give in the following the complete expressions for the widths used in the analysis. For tree-level widths we do not give here loop contributions and threshold effects, but those effects are taken into account in the numerical calculation of the branching ratios. The decays of a CP-even/odd neutral Higgs boson to a pair of fermions are:

invariance and are therefore model independent. There are no tree-level couplings of vector boson pairs to the charged Higgs  $H^\pm$  and to the CP-odd neutral Higgs boson  $A$ . For the neutral CP-even sector:

$$\Gamma(h^0 \rightarrow W^+ W^-) = \frac{\sin^2(\beta - \alpha)}{16\pi v^2 m_h} (m_h^4 - 4m_h^2 m_W^2 + 12m_W^4) \left(1 - 4\frac{m_W^2}{m_h^2}\right)^{1/2}, \quad (48)$$

$$\Gamma(h^0 \rightarrow ZZ) = \frac{\sin^2(\beta - \alpha)}{32\pi v^2 m_h} (m_h^4 - 4m_h^2 m_Z^2 + 12m_Z^4) \left(1 - 4\frac{m_Z^2}{m_h^2}\right)^{1/2}, \quad (49)$$

and the corresponding expressions for  $H^0$  can be obtained replacing  $\sin^2(\beta - \alpha)$  with  $\cos^2(\beta - \alpha)$ . The loop-induced decays to  $gg$  and  $\gamma\gamma$  can be obtained from chapter 2 and appendix C of the first reference in [1] for the MSSM. For a generic neutral Higgs boson  $\phi$  they are given by:

$$\Gamma(\phi^0 \rightarrow gg) = \frac{\alpha_s^2}{128\pi^3 v^2} m_\phi^3 \left| \sum_i J_i^\phi \right|^2, \quad (50)$$

$$\Gamma(\phi^0 \rightarrow \gamma\gamma) = \frac{\alpha_{em}^2}{256\pi^3 v^2} m_\phi^3 \left| \sum_i I_i^\phi \right|^2, \quad (51)$$

where the sum over the index  $i$  is limited to quarks for  $gg$

$$J_q^h = C_q^\phi F_{1/2}(\tau_q) \quad (52)$$

while it runs over fermions,  $W$ ,  $H^\pm$  for  $\gamma\gamma$ :

$$I_f^\phi = N_c e^2 C_f^\phi F_{1/2}(\tau_f) \quad (53)$$

$$I_W^\phi = C_W^\phi F_1(\tau_W) \quad (54)$$

$$I_{H^\pm}^\phi = C_{H^\pm}^\phi F_0(\tau_{H^\pm}) \frac{m_W^2}{m_{H^\pm}^2} \quad (55)$$

where  $\tau_i = 4m_i^2/m_\phi^2$ ,  $N_c = 3$  for quarks,  $N_c = 1$  for leptons,  $e$  is the electric charge in units of the charge of the electron, the functions  $F$  are given by

$$F_0 = \tau [1 - \tau g(\tau)] \quad (56)$$

$$F_{1/2} = -2\tau [\delta + (1 - \delta\tau)g(\tau)] \quad (57)$$

$$F_1 = 2 + 3\tau + 3\tau(2 - \tau)g(\tau) \quad (58)$$

where  $\delta = 1$  for  $h^0$ ,  $H^0$ , and  $\delta = 0$  for  $A$ . The function  $g(x)$  is

$$g(x) = \begin{cases} \text{asin}^2(\sqrt{1/x}) & x \geq 1 \\ -\frac{1}{4} \left[ \log \frac{1+\sqrt{1-x}}{1-\sqrt{1-x}} - i\pi \right] & x < 1 \end{cases} \quad (59)$$

The coefficients  $C_i^\phi$  are given in Table XII and the couplings  $g(h^0 H^+ H^-)$ ,  $g(H^0 H^+ H^-)$  of Table XII can be

TABLE XI: The mixing angles for the neutral Higgs bosons decays to fermions;  $u$  refers to up-type quarks,  $d$  to down-type quarks and leptons.

	MSSM	2HDM-III type a	2HDM-III type b
$\theta(h^0 \rightarrow u\bar{u})$	$\cos \alpha / \sin \beta$	$\cos \alpha / \sin \beta$	$\sin \alpha / \cos \beta$
$\theta(h^0 \rightarrow d\bar{d})$	$\sin \alpha / \cos \beta$	$\cos \alpha / \sin \beta$	$\sin \alpha / \cos \beta$
$\theta(h^0 \rightarrow \tau\mu)$	0	$\cos(\alpha - \beta) / (\sqrt{2} \sin \beta)$	$\cos(\alpha - \beta) / (\sqrt{2} \cos \beta)$
$\theta(H^0 \rightarrow u\bar{u})$	$\sin \alpha / \sin \beta$	$\sin \alpha / \sin \beta$	$\cos \alpha / \cos \beta$
$\theta(H^0 \rightarrow d\bar{d})$	$\cos \alpha / \cos \beta$	$\sin \alpha / \sin \beta$	$\cos \alpha / \cos \beta$
$\theta(H^0 \rightarrow \tau\mu)$	0	$\sin(\alpha - \beta) / (\sqrt{2} \sin \beta)$	$\sin(\alpha - \beta) / (\sqrt{2} \cos \beta)$
$\theta(A^0 \rightarrow u\bar{u})$	$\cot \beta$	$\cot \beta$	$\tan \beta$
$\theta(A^0 \rightarrow d\bar{d})$	$\tan \beta$	$\cot \beta$	$\tan \beta$
$\theta(A^0 \rightarrow \tau\mu)$	0	$1 / (\sqrt{2} \sin \beta)$	$1 / (\sqrt{2} \cos \beta)$

TABLE XII: The coefficients  $C_i^\phi$ ;  $u$  refers to up-type quarks,  $d$  to down-type quarks and leptons.

	2HDM-III type a	2HDM-III type b
$C_u^h$	$\cos \alpha / \sin \beta$	$-\sin \alpha / \cos \beta$
$C_d^h$	$\cos \alpha / \sin \beta$	$-\sin \alpha / \cos \beta$
$C_W^h$	$\sin(\beta - \alpha)$	$\sin(\beta - \alpha)$
$C_{H^\pm}^h$	$g(h^0 H^+ H^-)$	$g(h^0 H^+ H^-)$
$C_u^H$	$\sin \alpha / \sin \beta$	$\cos \alpha / \cos \beta$
$C_d^H$	$\sin \alpha / \sin \beta$	$\cos \alpha / \cos \beta$
$C_W^H$	$\cos(\beta - \alpha)$	$\cos(\beta - \alpha)$
$C_{H^\pm}^H$	$g(H^0 H^+ H^-)$	$g(H^0 H^+ H^-)$
$C_u^A$	$-\cot \beta$	$\tan \beta$
$C_d^A$	$\cot \beta$	$-\tan \beta$
$C_W^A$	0	0
$C_{H^\pm}^A$	0	0

found in Appendix A of the last paper in [27].

- 
- [1] J.F. Gunion, H.E. Haber, G.L. Kane, S. Dawson, The Higgs Hunter's Guide (Addison-Wesley, Reading, MA 1990), Erratum: arXiv:hep-ph/9302272; H. E. Haber and G. L. Kane, Phys. Rept. **117**, 75 (1985).
- [2] T. P. Cheng and M. Sher, Phys. Rev. D **35**, 3484 (1987); A. Antaramian, L. J. Hall and A. Rasin, Phys. Rev. Lett. **69**, 1871 (1992) [arXiv:hep-ph/9206205]; L. J. Hall and S. Weinberg, Phys. Rev. D **48**, 979 (1993) [arXiv:hep-ph/9303241]; M. J. Savage, Phys. Lett. B **266**, 135 (1991); M. E. Luke and M. J. Savage, Phys. Lett. B **307**, 387 (1993) [arXiv:hep-ph/9303249].
- [3] H. P. Nilles, Phys. Rept. **110**, 1 (1984).
- [4] G. F. Giudice and R. Rattazzi, Phys. Rept. **322**, 419 (1999) [arXiv:hep-ph/9801271].
- [5] R. Barbieri, G. R. Dvali and L. J. Hall, Phys. Lett. B **377**, 76 (1996) [arXiv:hep-ph/9512388].
- [6] L. J. Hall, V. A. Kostelecky and S. Raby, Nucl. Phys. B **267**, 415 (1986).
- [7] F. Borzumati and A. Masiero, Phys. Rev. Lett. **57**, 961 (1986).
- [8] J. Ellis, M. E. Gomez, G. K. Leontaris, S. Sola and D. V. Nanopoulos, hep-ph/9911459.
- [9] J. L. Feng, Y. Nir and Y. Shadmi, Phys. Rev. D **61** (2000) 113005 [arXiv:hep-ph/9911370].
- [10] J. Hisano, T. Moroi, K. Tobe and M. Yamaguchi, Phys. Rev. D **53** (1996) 2442 [arXiv:hep-ph/9510309]; Phys. Lett. B **391**, (1997) 341 [arXiv:hep-ph/9605296]; J. Hisano, D. Nomura and T. Yanagida, Phys. Lett. B **437** (1998) 351 [arXiv:hep-ph/9711348]; J. Hisano and D. Nomura, Phys. Rev. D **59** (1999) 116005 [arXiv:hep-ph/9810479]; J. Hisano, M. M. Nojiri, Y. Shimizu and M. Tanaka, Phys. Rev. D **60** (1999) 055008 [arXiv:hep-ph/9808410]; Phys. Rev. D **58**, (1998) 116010 [arXiv:hep-ph/9805367]; J. Hisano, hep-ph/9806222; J. Hisano, hep-ph/9906312; J. Hisano and K. Kurosawa, hep-ph/0004061.
- [11] M. Chaichian and K. Huitu, Phys. Lett. B **384**, 157 (1996) [arXiv:hep-ph/9603412]; K. Huitu, J. Maalampi, M. Raidal and A. Santamaria, Phys. Lett. B **430**, 355 (1998) [arXiv:hep-ph/9712249].
- [12] S. L. Glashow and S. Weinberg, Phys. Rev. D **15**, 1958 (1977).
- [13] D. Bowser-Chao, K. Cheung and W.-Y. Keung, Phys. Rev. D **59**, 115006 (1999) [arXiv:hep-ph/9811235].
- [14] G. Buchalla, A. Buras and M. Lautenbacher, Rev. Mod. Phys. **68**, 1125 (1996) [arXiv:hep-ph/9512380];

- A. J. Buras, M. Misiak, M. Munz and S. Pokorski, Nucl. Phys. **B424**, 374 (1994) [arXiv:hep-ph/9311345].
- [15] K. Chetyrkin, M. Misiak and M. Munz, Phys. Lett. **B400**, 206 (1997); Erratum-ibid. **B425**, 414 (1998) [arXiv:hep-ph/9612313]; M. Ciuchini, G. Degrassi, P. Gambino and G. F. Giudice, Nucl. Phys. **B527**, 21 (1998) [arXiv:hep-ph/9710335]; A. Kagan and M. Neubert, Eur. Phys. J. C **7**, 5 (1999).
- [16] M. S. Alam, CLEO Collaboration, Phys. Rev. Lett. **74**, 2885 (1995); R. Briere, in Proceedings of ICHEP98, Vancouver, Canada 1998, CLEO-CONF-98-17; and in talk by J. Alexander, *ibid.*
- [17] R. Barate, ALEPH Collaboration, Phys. Lett. B **429**, 169 (1998).
- [18] J. L. Hewett, Phys. Rev. Lett. **70**, 1045 (1993) [arXiv:hep-ph/9211256]; V. D. Barger, M. S. Berger and R. J. Phillips, Phys. Rev. Lett. **70**, 1368 (1993) [arXiv:hep-ph/9211260]; F. M. Borzumati and C. Greub, Phys. Rev. D **58**, 074004 (1998) [arXiv:hep-ph/9802391]; J. A. Coarasa, J. Guasch, J. Sola and W. Hollik, Phys. Lett. B **442**, 326 (1998) [arXiv:hep-ph/9808278]; F. M. Borzumati and C. Greub, Phys. Rev. D **59**, 057501 (1999) [arXiv:hep-ph/9809438]; G. Degrassi, P. Gambino and G. F. Giudice, JHEP **0012**, 009 (2000) [arXiv:hep-ph/0009337]; P. Gambino and M. Misiak, Nucl. Phys. B **611**, 338 (2001) [arXiv:hep-ph/0104034].
- [19] A. Atwood, L. Reina and A. Soni, Phys. Rev. D **55**, 3156 (1997), [arXiv:hep-ph/9609279].
- [20] J. L. Diaz Cruz, J. J. Godina Nava and G. Lopez Castro, Phys. Rev. D **51**, 5263 (1995) [arXiv:hep-ph/9509229].
- [21] M. Sher and Y. Yuan, Phys. Rev. D **44**, 1461 (1991).
- [22] S. Nie and M. Sher, Phys. Rev. D **58**, 097701 (1998) [arXiv:hep-ph/9805376].
- [23] H. N. Brown *et al.* [Muon g-2 Collaboration], Phys. Rev. Lett. **86**, 2227 (2001) [arXiv:hep-ex/0102017]; G. W. Bennett *et al.* [Muon g-2 Collaboration], arXiv:hep-ex/0208001.
- [24] M. Knecht and A. Nyffeler, arXiv:hep-ph/0111058; M. Knecht, A. Nyffeler, M. Perrottet and E. De Rafael, Phys. Rev. Lett. **88**, 071802 (2002) [arXiv:hep-ph/0111059]; I. Blokland, A. Czarnecki and K. Melnikov, Phys. Rev. Lett. **88**, 071803 (2002) [arXiv:hep-ph/0112117]; J. Bijnens, E. Pallante and J. Prades, Nucl. Phys. B **626**, 410 (2002) [arXiv:hep-ph/0112255].
- [25] M. Ramsey-Musolf and M. B. Wise, arXiv:hep-ph/0201297.
- [26] J. P. Leveille, Nucl. Phys. B **137**, 63 (1978).
- [27] H. E. Haber and R. Hempfling, Phys. Rev. Lett. **66**, 1815 (1991); J. R. Ellis, G. Ridolfi and F. Zwirner, Phys. Lett. B **257**, 83 (1991); Y. Okada, M. Yamaguchi and T. Yanagida, Prog. Theor. Phys. **85**, 1 (1991); H. E. Haber, arXiv:hep-ph/9707213.
- [28] J. A. Aguilar-Saavedra and G. C. Branco, Phys. Lett. B **495**, 347 (2000) [arXiv:hep-ph/0004190].
- [29] S. Bejar, J. Guasch and J. Sola, in *Proc. of the 5th International Symposium on Radiative Corrections (RADCOR 2000)* ed. Howard E. Haber, arXiv:hep-ph/0101294.
- [30] T. Han, J. Jiang and M. Sher, Phys. Lett. B **516**, 337 (2001) [arXiv:hep-ph/0106277].
- [31] Y. Fukuda *et al.* [SuperKamiokande Collaboration], Phys. Rev. Lett. **82**, 2644 (1999) [arXiv:hep-ex/9812014]; **85**, 3999 (2000) [arXiv:hep-ex/0009001]; **86**, 5656 (2001) [arXiv:hep-ex/0103033].
- [32] L. Serin and R. Stroynowski, ATLAS Internal Note, ATL-PHYS-97-114 (1997).
- [33] I. Hinchliffe and F. E. Paige, Phys. Rev. D **63**, 115006 (2001) [arXiv:hep-ph/0010086].
- [34] J. L. Diaz-Cruz and J. J. Toscano, Phys. Rev. D **62**, 116005 (2000) [arXiv:hep-ph/9910233].
- [35] M. Sher, Phys. Lett. B **487**, 151 (2000) [arXiv:hep-ph/0006159].
- [36] U. Cotti, L. Diaz-Cruz, C. Pagliarone and E. Vataga, in *Proc. of the APS/DPF/DPB Summer Study on the Future of Particle Physics (Snowmass 2001)* ed. R. Davidson and C. Quigg, arXiv:hep-ph/0111236.
- [37] A. Djouadi, J. Kalinowski and M. Spira, Comput. Phys. Commun. **108**, 56 (1998) [arXiv:hep-ph/9704448].
- [38] T. Sjöstrand, Comput. Phys. Commun. **82**, 74 (1994); T. Sjöstrand, P. Eden, C. Friberg, L. Lonnblad, G. Miu, S. Mrenna and E. Norrbin, Comput. Phys. Commun. **135**, 238 (2001) [arXiv:hep-ph/0010017]; T. Sjöstrand, L. Lonnblad and S. Mrenna, arXiv:hep-ph/0108264.
- [39] H. L. Lai *et al.*, Phys. Rev. D **55**, 1280 (1997) [arXiv:hep-ph/9606399].
- [40] E. Richter-Was, D. Froidevaux and L. Poggioli, ATLAS Internal Note, ATL-PHYS-98-131, (1998).
- [41] M. Spira, hep-ph/9510347.
- [42] S. Balatenychev *et al.*, 'Theoretical Developments', in [53], p.4; and the references therein.
- [43] S. Catani, D. de Florian and M. Grazzini, JHEP **0201**, 015 (2002) [arXiv:hep-ph/0111164].
- [44] S. Frixione, P. Nason and G. Ridolfi, Nucl. Phys. B **383**, 3 (1992); S. Frixione, Nucl. Phys. B **410**, 280 (1993); U. Baur, T. Han and J. Ohnemus, Phys. Rev. D **48**, 5140 (1993) [arXiv:hep-ph/9305314]; Phys. Rev. D **51**, 3381 (1995) [arXiv:hep-ph/9410266]; Phys. Rev. D **53**, 1098 (1996) [arXiv:hep-ph/9507336]; Phys. Rev. D **57**, 2823 (1998) [arXiv:hep-ph/9710416].
- [45] L. J. Dixon, Z. Kunszt and A. Signer, Phys. Rev. D **60**, 114037 (1999) [arXiv:hep-ph/9907305].
- [46] J. Campbell and R. K. Ellis, <http://theory.fnal.gov/people/ellis/Programs/mcfm.html>, arXiv:hep-ph/0202176.
- [47] S. Jadach, Z. Was, R. Decker and J. H. Kühn, Comput. Phys. Commun. **76**, 361 (1993); M. Jezabek, Z. Was, S. Jadach and J. H. Kühn, Comput. Phys. Commun. **70**, 69 (1992); S. Jadach, J. H. Kühn and Z. Was, Comput. Phys. Commun. **64**, 275 (1990).
- [48] T. Han and D. Marfatia, Phys. Rev. Lett. **86**, 1442 (2001) [arXiv:hep-ph/0008141].
- [49] D. Rainwater, D. Zeppenfeld and K. Hagiwara, Phys. Rev. D **59**, 014037 (1999) [arXiv:hep-ph/9808468]; L. Di Lella, Proceedings of the large Hadron Collider Workshop, Aachen, Vol II, p.183, 1990, edited by G. Jarlskog and D. Rein, CERN 90-10/ECFA 90-133.
- [50] ATLAS Collaboration, 'ATLAS Detector and Physics Performance Technical Design Report', CERN/LHCC/99-15, 742 (1999); D. Cavalli *et al.*, ATLAS Internal Note ATL-PHYS-94-051; D. Cavalli *et al.*, 'Study of the MSSM channel  $A/H \rightarrow \tau\tau$  at the LHC', in [53], p.67.
- [51] R. Kinnunen and D. Denegri, CMS NOTE 1999/037, arXiv:hep-ph/9907291; A. Nikitenko, S. Kunori and R. Kinnunen, CMS Note 2001/040; D. Denegri *et al.*, CMS NOTE 2001/032, arXiv:hep-ph/0112045.
- [52] R. A. Diaz, R. Martinez and J. Alexis Rodriguez, Phys. Rev. D **63**, 095007 (2001); Phys. Rev. D **64**, 033004

(2001) [arXiv:hep-ph/0103050].  
[53] D. Cavalli *et al.*, “The Higgs working group: Summary

report,” arXiv:hep-ph/0203056.